Redox Biology 62 (2023) 102702

Contents lists available at ScienceDirect

Redox Biology

journal homepage: www.elsevier.com/locate/redox

BNP protects against diabetic cardiomyopathy by promoting Opa1-mediated mitochondrial fusion via activating the PKG-STAT3 pathway

Pan Chang [a,b,1], Xiaomeng Zhang [c,1], Jing Zhang [a,1], Jianbang Wang [a], Xihui Wang [a], Man Li [a,d], Rui Wang [a], Jun Yu [b,**], Feng Fu [d,e,*]

[a] Department of Cardiology, The Second Affiliated Hospital, Xi'an Medical University, Xi'an, Shaanxi, 710038, China
[b] Clinical Experimental Center, The Affiliated Xi'an International Medical Center Hospital, Northwest University, Xi'an, 710100, China
[c] Department of Cardiology, Xijing Hospital, Air Force Medical University, 169 Changle West Road, Xi'an, 710032, China
[d] Department of Physiology and Pathophysiology, National Key Discipline of Cell Biology, Air Force Medical University, Xi'an, 710032, China
[e] Department of Cardiology, Tangdu Hospital, Airforce Medical University, Xi'an, 710038, China

ARTICLE INFO

Keywords:
Diabetic cardiomyopathy
Brain natriuretic peptide
Mitochondrial fusion
PKG
STAT3

ABSTRACT

Brain natriuretic peptide (BNP) belongs to the family of natriuretic peptides, which are responsible for a wide range of actions. Diabetic cardiomyopathy (DCM) is often associated with increased BNP levels. This present research intends to explore the role of BNP in the development of DCM and the underlying mechanisms. Diabetes was induced in mice using streptozotocin (STZ). Primary neonatal cardiomyocytes were treated with high glucose. It was found that the levels of plasma BNP started to increase at 8 weeks after diabetes, which preceded the development of DCM. Addition of exogenous BNP promoted Opa1-mediated mitochondrial fusion, inhibited mitochondrial oxidative stress, preserved mitochondrial respiratory capacity and prevented the development of DCM, while knockdown of endogenous BNP exacerbated mitochondrial dysfunction and accelerated DCM. Opa1 knockdown attenuated the aforementioned protective action of BNP both *in vivo* and *in vitro*. BNP-induced mitochondrial fusion requires the activation of STAT3, which facilitated Opa1 transcription by binding to its promoter regions. PKG, a crucial signaling biomolecule in the BNP signaling pathway, interacted with STAT3 and induced its activation. Knockdown of NPRA (the receptor of BNP) or PKG blunted the promoting effect of BNP on STAT3 phosphorylation and Opa1-mediated mitochondrial fusion. The results of this study demonstrate for the first time that there is a rise in BNP during the early stages of DCM as a compensatory protection mechanism. BNP is a novel mitochondrial fusion activator in protecting against hyperglycemia-induced mitochondrial oxidative injury and DCM through the activation of NPRA-PKG-STAT3-Opa1 signaling pathway.

1. Introduction

The prevalence of diabetes mellitus has been growing rapidly over many years. Based on the most recent data, the number of diabetic patients was predicted to reach 693 million by 2045 all over the world [1]. Cardiovascular complications associated with diabetes are a leading cause for morbidity and mortality [2]. Diabetic cardiomyopathy (DCM) is a diabetes-related cardiac condition that is characterized by ventricular dysfunction without coronary artery disease or hypertension [3]. The underlying pathogenesis of DCM has not yet been fully defined.

BNP is a cardiac hormone mainly secreted by ventricular cardiomyocytes, it has vasodilatory properties and helps to reduce the preload and afterload. BNP has been considered as an inhibitor of myocardial hypertrophy [4,5] as well as fibrosis [6], and a protector against myocardial ischemia-reperfusion injury [7]. Food and Drug Administration (FDA) has approved human recombinant BNP (nesiritide) for treating acute decompensated congestive heart failure [8]. Previous research findings have shown that DCM is often accompanied by upregulated cardiac BNP gene expression and increased serum BNP levels in animal experiments [9–11]. However, it remains unclear when

* Corresponding author. Department of Physiology and Pathophysiology, National Key Discipline of Cell Biology, Air Force Medical University, China.
** Corresponding author. Clinical Experimental Center, The Affiliated Xi'an International Medical Center Hospital, Northwest University, China.
E-mail addresses: pclamper@163.com (J. Yu), fufeng048@126.com (F. Fu).
[1] Pan Chang, Xiaomeng Zhang and Jing Zhang contributed equally to this study.

https://doi.org/10.1016/j.redox.2023.102702
Received 21 February 2023; Received in revised form 25 March 2023; Accepted 14 April 2023
Available online 20 April 2023

BNP levels start to increase during the development of DCM. Moreover, the role of elevated BNP in DCM progression is not well understood.

The heart is an energy-consuming organ, largely dependent on mitochondrial function, which provides about 90% of its energy. Mitochondrial dynamics, including the processes of mitochondrial fusion and fission, performs a crucial function in maintaining the mitochondria's optimum efficiency [12]. Abnormal mitochondrial dynamics is involved in the pathogenisis of many cardiac diseases including DCM. It is known that mitochondrial fusion is beneficial since it increases mitochondrial function as well as the production of ATP [13]. Conversely, excessive mitochondrial fission may be detrimental because it results in mitochondrial dysfunction and increased ROS [14]. Nevertheless, it is still largely unknown whether BNP has a regulatory effect on imbalanced mitochondrial dynamics under hyperglycaemic conditions.

Herein, we find that increased plasma BNP precedes the development of DCM in both diabetic animals and patients. Addition of exogenous BNP prevents the development of DCM by stimulating Opa1-mediated mitochondrial fusion through PKG-STAT3 pathway, while knockdown of endogenous BNP exacerbates mitochondrial dysfunction and accelerated DCM.

2. Materials and methods

2.1. Animal experiments and human study

This research followed National Institutes of Health (NIH) criteria for the Care and Use of Laboratory Animals (8th Edition, 2011). All experiments involving animals and human subjects were approved by the Ethics Committee of the Second Affiliated Hospital of Xi'an Medical University (Approval No. MR-61-22-020,655). Male 8-week-old C57BL/6 mice were injected with streptozotocin (50 mg/kg/d) intraperitoneally for five successive days [15]. Prior to STZ injection, mice were anaesthetized with isofluorane. A week following the last administration of STZ, experimental animals with fasting glucose levels >11.1 mmol/L were determined to develop diabetes. Mice serving as controls had a similar injection of vehicle every day. A total number of 192 mice were included in this study. Vehicle or BNP (GenScript, Piscataway, NJ, USA) was randomly assigned and was administered to control or diabetic mice for 4 weeks using subcutaneous osmotic pumps at a rate of 0.25 μL/h (Alzet, model 2004; Cupertino, CA, USA). All experimental models were placed in conventional settings (12h/12h light/dark cycle) and fed a recommended mouse chow with ad libitum access to water. Animals were anaesthetized by 3% isoflurane and maintained with 1% isoflurane via inhalation. Euthanasia was carried out using carbon dioxide, in accordance with the AVMA Guidelines for the Euthanasia of Animals 80 (2020) and with the approval of local animal welfare committees.

The human study was performed in adherence to the Declaration of Helsinki. Patients with newly diagnosed diabetes were enrolled in this study. They had not received any anti-diabetic treatment before enrollment. Diabetes was diagnosed according to World Health Organization (WHO) criteria, all subjects provided written informed consent. Participants with coronary artery disease, hypertrophic cardiomyopathies, restrictive cardiomyopathies, dilated cardiomyopathies, arrhythmogenic right ventricular dysplasia, or other micro-or macrovascular consequences of diabetes were excluded from the current study. Additionally, patients with renal failure, serious psychological problems and cancer were excluded. Final enrollment included 30 control volunteers, 30 diabetics, and 30 diabetics with DCM. The plasma samples were obtained and kept at −80 °C. The patient data were included in Supplemental Table S1.

2.2. Echocardiography

Echocardiography was performed in M-mode using VEVO 2100 system (Visual Sonics, Toronto, Canada) [14]. Mice were anaesthetized with isoflurane. By controlling the flow of isoflurane, the heart rate of the mice was limited to 400–500 beats/min as recommended. The images of left ventricular (LV) dimensions were recorded to measure left ventricular ejection fraction (LVEF) and left ventricular fractional shortening (LVFS).

2.3. Biochemical and histological analysis

An automated biochemical analyzer was used to determine the levels of blood glucose, total cholesterol (TC), and triacylglycerol (TG) in fasting plasma (Chemray 800, Rayto, China). We measured plasma BNP concentrations using an ELISA kit (Raybiotech, Norcross, GA, USA). PKG activity assays were performed using the PKG Kinase Enzyme assay kit from Promega.

Heart morphology were stained with hematoxylin and eosin (Beyotime, Jiangsu, China). Staining cardiomyocytes with FITC-labeled WGA (Servicebio, Wuhan, China) allowed us to determine their cross-sectional area. Masson's trichrome stain (Servicebio, Wuhan, China) was used to examine the myocardium's interstitial fibrosis.

2.4. Measurement of blood pressure

Systolic blood pressure and diastolic blood pressure was measured using the non-invasive tail-cuff system (Kent scientific corporation, Torrington, CT, USA). Briefly, mice were placed on the pre-warmed platform (30 °C) and tails were inserted into the tail cuffs for 5 consecutive days. At each session, at least 10 reads were obtained and averaged as the blood pressure at that time point.

2.5. Transmission electron microscopy (TEM)

The cardiac tissues were fixed in a 2.5% glutaraldehyde and 1% cacodylate buffer at pH 7.4 for 2 days at 4 °C. The tissues were first rinsed several times with 0.1 M cacodylate buffer, followed by the addition of 0.1% tannic acid to deionized water, and finally osmium tetroxide to deionized water. The detailed steps were carried out as described before [14]. An image of each slice was taken with a charge-coupled device (CCD) camera equipped with a JEM-1230 TEM (JEOL Ltd., Tokyo, Japan). The mitochondrial images were analyzed using Image J software.

2.6. Cell culture

Primary cardiomyocytes were separated from the hearts of neonatal Sprague-Dawley mice via collagenase I (gibco) digestion, as previously described [16]. Cells were cultured in Dulbecco's modified Eagle's medium (DMEM) containing 10% fetal bovine serum (FBS) and normal glucose (5.5 mmol/L, NG). Cardiomyocytes were exposed to normal glucose (5.5 mmol/L, NG) or HG (33 mmol/L, HG) for 48 h [17] with the vehicle or BNP supplement.

2.7. Mitochondrial morphology in the cardiomyocytes

To assess mitochondrial morphology in the cardiomyocytes, the mitochondria were stained using the fluorescent probe MitoTracker Green FM (Ex/Em: 490/516 nm, M7514, Invitrogen, USA) in accordance with the methods of the manufacture. The cardiomyocytes were plated in a confocal dish and treated with 50 nM MitoTracker Green FM for 30 min. We examined the images under a confocal laser scanning microscope (Nikon A1R MP + Confocal Microscope, Nikon, Japan) and analyzed mitochondrial morphology as previously described [18].

2.8. Measurement of mitochondrial membrane potential

As described previously [19], we measured the mitochondrial membrane potential using JC-1 dye from Beyotime (Jiangsu, China). FACScan flow cytometry (BD Facscalibur, Franklin Lakes, NJ, USA) was

used to measure the fluorescence of JC-1 after incubation of primary cardiomyocytes at 37 °C for 15 min with 1.0 μM JC-1.

2.9. Quantitative real-time PCR (RT-qPCR)

RT-qPCR was used to detect the gene expression levels for Opa1 and the relative mtDNA content to nuclear DNA content as described previously [20,21]. The primer sequences were: Opa1 forward CAACCCCGCAGGAACTTTTG; reverse GGTGTACCCGCAGTGAAGAA; mtDNA forward AACATACGAAAAACACACCCATT; reverse AGTGTATGGCTAAGAAAAGACCTG; β-actin forward CCCTGGCTCCTAGCACCAT; reverse AGAGCCACCAATCCACACAGA.

2.10. Reactive oxygen species (ROS) generation in the cardiomyocytes and hearts

Cardiomyocytes were seeded in a confocal dish and were loaded with 5 μM MitoSOX Red or CM-H2DCFDA (Thermo Fisher Scientific, Waltham, MA, USA) for 10 min in the dark at 37 °C. After several washes, images were visualized under a confocal laser-scanning microscope (Nikon A1R MP + Confocal Microscope, Nikon, Japan).

Dihydroethidium (DHE) staining was used previously to assess the production of superoxide anion in mouse heart tissue [16]. Briefly, 2 μmol/L fluorescent dye DHE (Thermo Fisher Scientific, Waltham, MA, USA) was added to the 6 μm thick snap-frozen heart sections and incubated at 37 °C for 30 min in a humidified dark chamber. ImageJ analysis software was used to analyze the DHE-positive cells. MnSOD activity was measured using MnSOD assay kits (S1013, Beyotime Biotechnology, Jiangsu, China) according to the manufacturer's protocol.

Oxidative stress from superoxide was also measured by a modified HPLC-based method to quantify 2-OH-ethidium and ethidium levels as previously described [22]. Briefly, before the start of the experiment, increasing concentrations of 2-OH-ethidium and ethidium were loaded onto the column to generate a standard curve. Tissues were incubated with 50 μM DHE for 30 min at 37 °C in PBS buffer. Following several rounds of washing with Krebs solution buffered with 10 mM HEPES-NaOH (pH 7.4), tissues were frozen with liquid nitrogen and pulverized. The supernatant was analyzed using an HPLC system with a JASCO FP-1520 fluorescence detector and a Beckman ultrasphere reverse column (C18). Similar to DHE, MitoSOX oxidation products (Mito-2-OH-ethidium and Mito-ethidium) were separated using a C18 reverse-phase column and measured using HPLC.

2.11. Mitochondrial oxygen consumption rate (OCR) analysis

Mitochondrial respiratory activity was measured employing an XF24 Extracellular Flux Analyzer (Agilent Seahorse Bioscience, Santa Clara, CA, USA). Primary cardiomyocytes were seeded at 2×10^4 per well in the XF24 Cell Culture Microplate. We used Seahorse XF Cell Mito Stress Test Kit (Agilent Technologies, Santa Clara, CA, USA) to record the OCR with sequential injection of 1 μM oligomycin A, 1 μM FCCP, and 0.5 μM antimycin A [23]. Pierce BCA Protein Assay Kit (Thermo Fisher Scientific, Waltham, MA, USA) was used to adjust all raw results to the protein content.

2.12. Transfection of siRNAs against BNP, Opa1, STAT3, PKG and NPRA

SiRNAs against BNP (#sc-62023, Santa Cruz Biotechnology), Opa1 (sense: CCAGCAAGGUUAGCUGCAATT; antisense: UUGCAGCUAACCUUGCUGGTT), STAT3 (#sc-270,027, Santa Cruz Biotechnology), PKG (sense: CGAAGAUUCUCAUGCUCAA; antisense: UUGAGCAUGAGAAUCUUCG), NPRA (#sc-40126, Santa Cruz Biotechnology) and negative control siRNA were transfected into primary cardiomyocytes by using Lipofectamine RNAiMAX reagent (Invitrogen). Following 48 h of transfection, cells were used for subsequent tests in NG or HG media.

2.13. Assay for apoptotic cell death

Using Annexin V-FITC and PI apoptosis detection kits (BD Biosciences, CA, USA), the apoptotic frequency of primary cardiomyocytes was determined by flow cytometry. A terminal deoxynucleotidyl transferase-UTP nick end labeling (TUNEL) assay kit (Roche Applied Science, Penzberg, Germany) and the caspase-3 activity test kit (KeyGEN Biotech, Jiangsu, China) were used to evaluate apoptotic rate in cardiac tissues according to the manufacturer's recommendations. Confocal fluorescence microscopy (Leica, Heerbrugg, Switzerland) was used to evaluate the TUNEL and DAPI-stained slices.

2.14. Adeno-associated virus transfection in vivo

For the Opa1 or BNP knockdown studies *in vivo*, adeno-associated viral (AAV) vectors carrying a scrambled sequence (AAV-Con) or a short hairpin RNA (shRNA) directed against the mouse Opa1 RNA (AAV-Opa1-shRNA) or BNP RNA (AAV-BNP-shRNA) were constructed by Hanbio Biotechnology (Shanghai, China). Isoflurane (2.5%) was used to anesthetize the mouse models, and the hearts were exposed. A total amount of 40 μL (approximately 1×10^{11} PFU/ml) AAV-Con shRNA, AAV-Opa1-shRNA, or AAV-BNP-shRNA was injected at four different sites of each left ventricle free wall, as we have described previously [16]. The mice were administered with STZ (50 mg/kg/d) intraperitoneally for 5 consecutive days one week after transfection to establish a diabetes model [15], and then the vehicle or BNP was administered.

2.15. Western blotting and dot blot

Total proteins in mouse heart tissue or primary cardiomyocytes were determined with a Bradford protein assay (Beyotime, Jiangsu, China) on lysates obtained with RIPA (Beyotime, Jiangsu, China). Protein expression and modification was assessed by standard Western blot analysis. The extracted proteins were electrophoresed on SDS-PAGE and transferred to PVDF membranes. After blocked with 5% milk, the membranes were incubated with primary antibodies under 4 °C overnight. β-actin was used as the loading control. The detailed information of all the antibodies used has been provided in Supplementary Table S2. Afterwards, the membrane was treated with an anti-rabbit or anti-mouse secondary antibody that had been coupled with horseradish peroxidase (#A0208, #A0216, Beyotime Biotechnology, Jiangsu, China) at room temperature for 1 h and the blot was exposed by Supersignal chemiluminescence detection kit (Thermo Fisher Scientific, Waltham, MA, USA).

The oxidative stress markers including malondialdehyde (MDA), hydroxynonenal (HNE) and 3-nitrotyrosine (3NT) positive proteins were assessed by dot blot analysis referring to previous studies [24,25]. Cardiac protein homogenates were transferred to nitrocellulose membranes. A mouse monoclonal MDA antibody (abcam #ab243066, UK), a rabbit polyclonal 4-HNE antibody (abcam #ab46545, UK) and a mouse monoclonal 3-NT antibody (abcam #ab61392, UK) were used for dot blot analysis. Detection and quantification of all blots was performed by ECL with peroxidase conjugated anti-rabbit or anti-mouse secondary antibody (#A0208, #A0216, Beyotime Biotechnology, Jiangsu, China). The blot densities were analyzed by Quantity One software (Bio-Rad, San Diego, CA, USA).

2.16. Chromatin immunoprecipitation (ChIP) analysis

A Simple ChIP Plus Enzymatic Chromatin IP kit (#9005; Cell Signaling Technology, Danvers, USA) was used to perform ChIP in accordance with the manufacturer 's recommendations as described in our previously report [26]. Briefly, after fixation with 1% formaldehyde, the cardiomyocytes were homogenized in lysis buffer. Following that,

antibodies against STAT3 (#12640, Cell Signaling Technology) and protein G magnetic beads were added. Normal IgG was used as the negative control. DNA was extracted from the precipitation and then analyzed using primers for the Opa1 promoter (forward: 5′-TCCAGTTAGGTTTTGGGCCTT-3′ and reverse: 5′-TCCTTTTATGAGCCCCAATTTCCTT-3′) in RT-qPCR.

2.17. Co-immunoprecipitation assays

Co-immunoprecipitation was performed using the Pierce Co-Immunoprecipitation Kit (Thermo Fisher Scientific, Rockford, IL, USA) as described previously [27]. Briefly, the cells were prepared in Lysis/Wash Buffer, and 1 mg protein lysate was incubated overnight with 5 μg specific antibodies at 4 °C. The immunocomplexes were precipitated and performed with agarose resin slurry for 1 h. Those beads were washed and then subjected to Western blot procedures.

2.18. Statistical analysis

All the data are expressed as the mean ± SEM. For the statistical analysis of two groups, the unpaired Student's t-test was used. More than two groups were compared using one-way analysis of variance (ANOVA) or two-way ANOVA followed by Bonferroni's multiple comparison tests using GraphPad Prism 8.0. P values less than 0.05 were considered statistically significant.

3. Results

3.1. Increased plasma BNP level preceded the occurrence of DCM

Plasma BNP concentration was detected during the development of DCM. As shown in Supplementary Figs. S1A–B, plasma BNP concentration was increased at 8 weeks after the onset of diabetes in the diabetic mice, while diabetic cardiomyopathy occurs when cardiac function was significantly impaired (as evidenced by decreased LVEF) at 12 weeks after the onset of diabetes. Thus, BNP elevation (8 weeks after diabetes) was detectable before diabetic cardiomyopathy (12 weeks after diabetes) in the mice. Clinical characteristics of human subjects were provided in Supplementary Table S1. Compared with healthy controls or diabetic patients, DCM patients exhibited reduced LVEF (Supplementary Fig. S1D). BNP was much higher in the DCM group (440.85 ± 45.72 pg/ml) than in the healthy control (30.10 ± 4.00 pg/ml) or DM group (69.73 ± 6.48 pg/ml) (Supplementary Fig. S1C). Despite considering the differences in average age between the groups (50 vs 55 vs 62), BNP remained significantly elevated in the DCM group. Human plasma BNP contents in the DM group in Fig. S1C correspond to animal plasma BNP contents at 0–4 weeks of diabetes in Fig. S1A. At this stage, even though diabetes is induced, cardiac ejection fraction is still preserved and plasma BNP is unchanged. Pearson analysis indicated that there was no significant correlation between BNP level and fasting plasma glucose in diabetic patients with or without cardiac dysfunction ($R^2 = 0.0097$, $P = 0.49$, Supplementary Fig. S1E).

To explore the effects of increased BNP on DCM, exogenous BNP was administered to the mice according to the elevated level of plasma BNP during the development of DCM. The mice were administrated with BNP at 0.75, 1.5 or 3 μg/kg/h using subcutaneous osmotic pumps. The ELISA assay showed that 0.75 μg/kg/h BNP administration increased plasma BNP level to approximately 75 pg/ml (Supplementary Fig. S2), which are comparable to increased BNP levels at 8 weeks after diabetes in mice as aforementioned above. Therefore, the mice were treated with 0.75 μg/kg/h BNP for a 4-week period beginning at 8 weeks after diabetes.

3.2. BNP administration alleviated diabetic cardiomyopathy in the mice

Compared with control mice, diabetic mice had reduced body weight along with elevated blood glucose, food intake, serum total cholesterol (TC), triacylglycerol (TG) levels and blood pressure (Supplementary Table S3). These metabolic indicators were not affected by BNP treatment. As shown in Fig. 1A–C, diabetic animals exhibited decreased cardiac function, as shown by lower LVEF and LVFS than control animals. BNP therapy enhanced cardiac performance in the diabetic animals (Heart rate: Con 444.5 ± 10.22 bpm, Con + BNP 438.1 ± 9.95 bpm, DM 438.8 ± 11.55 bpm, DM + BNP 437.0 ± 10.50 bpm).

Hypertrophy and fibrosis of the heart are common features in DCM. As shown in Fig. 1D–G, diabetic animals exhibited significant cardiac hypertrophy and fibrosis, as evidenced by hypertrophied myocardium (Fig. 1D, HE staining), increased cardiomyocyte cross-sectional area (WGA staining in Fig. 1D and F), elevated heart weight-to-tibia length ratios (Fig. 1E), and intensived interstitial fibrosis (Fig. 1G) in comparison to control hearts. BNP administration dramatically ameliorated the pathological changes in the diabetic heart. The pathogenesis of DCM is often associated with cardiomyocyte apoptosis and oxidative stress. As expected, myocardial apoptotic markers such as the apoptotic index and caspase-3 activation were elevated in diabetic hearts relative to normal hearts. Treatment with BNP significantly reduced the apoptosis indicators in the diabetic hearts (Fig. 2A–C). Moreover, the production of DHE was greater in the diabetic hearts than the control hearts (Fig. 2D and E), while MnSOD activity was reduced in diabetic hearts (Fig. 2I). The changes of oxidative stress mentioned above could be reversed by BNP treatment. BNP also prevented the increase in DHE-derived oxidation products (2-OH-ethidium and ethidium) induced by diabetes (Fig. 2F–H). The oxidative stress markers including MDA, HNE and 3NT positive proteins were found at higher levels in the diabetic hearts and decreased by BNP treatment (Fig. 2J-L). These findings demonstrated that BNP reduced diabetes-induced oxidative stress, apoptosis, and improved cardiac structure and function in diabetic mice. Altogether, these findings suggest that BNP treatment could prevent the development of DCM. Correspondingly, it was found that the protein expression of natriuretic peptide receptor A (NPRA, the receptor of BNP) was largely preserved (approximately 75% of con) at 8 weeks after diabetes (Supplementary Figs. S3A–B), while at 12 weeks after diabetes, NPRA expression was significantly reduced (approximately 20% of con, Supplementary Figs. S3A–B). Furthermore, HG treatment time-dependently reduced NPRA expression in the cardiomyocytes (Supplementary Figs. S3C and D).

3.3. BNP treatment increased mitochondrial fusion and alleviated mitochondrial dysfunction in DCM

Next, the mechanisms underlying the cardioprotective effects of BNP treatment were explored. Mitochondrial morphological analysis showed that the number of mitochondria per μm^2 was not changed among all the groups, while mean mitochondrial size was significantly decreased in diabetic hearts compared to control hearts (Fig. 3A–G). BNP treatment increased mean size of the mitochondria in diabetic hearts (Fig. 3C). Fig. 3D showed that BNP inhibited the diabetes-induced reduction of ATP. The protein expression of PCG1α, an important transcription factor for maintaining mitochondrial biogenesis, was not significantly changed in diabetic hearts (Fig. 3E). The proteins related to mitochondrial fusion (Mfn1, Mfn2, and Opa1) as well as mitochondrial fission (Drp1 and Fis1) were assessed. Mfn1, Mfn2, Drp1, as well as Fis1 showed no significant variations in the levels among all the groups, only Opa1 was significantly reduced in diabetic hearts. Treatment with BNP prevented the decrease in Opa1 caused by diabetics (Fig. 3E and F). Additionally, BNP reversed the decline in Opa1 mRNA expression (Fig. 3G).

The action of BNP on the hearts and mitochondria *in vivo* may be affected by its systemic effects. To determine the direct effects of BNP on the heart, the cardiomyocytes were incubated with NG or HG medium for 48 h containing 75 pg/ml BNP *in vitro*, which was comparable with the concentration of plasma BNP at 8 weeks after diabetes *in vivo*. As shown in Supplementary Figs. S4A–D, BNP remarkably reduced the cell apoptosis rate and increased mitochondrial membrane potential in HG-

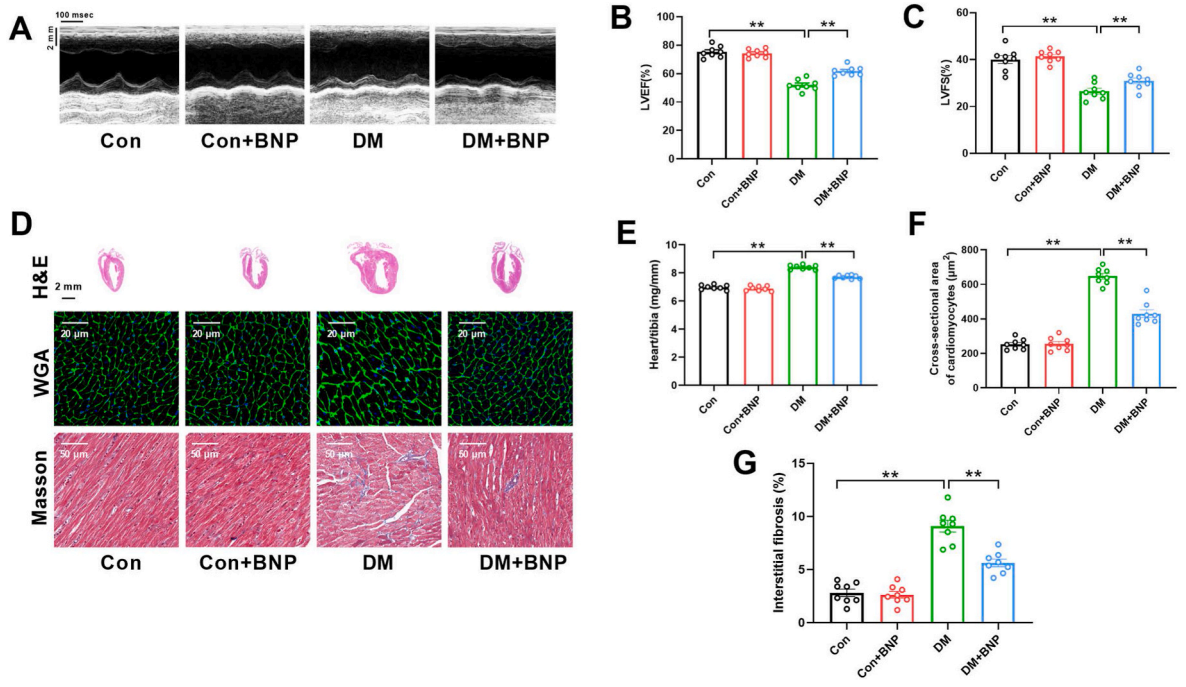

Fig. 1. BNP treatment alleviated cardiac functional and structural abnormalities in diabetic hearts. (A) Representative M-mode echocardiography images. (B) Left ventricular ejection fraction (LVEF). (C) Left ventricular fractional shortening (LVFS). (D) Stainings of hematoxylin and eosin, wheat germ agglutinin (WGA), and Masson trichrome. (E) The ratio of heart weight to tibia length. (F) Cardiomyocyte cross-sectional area. (G) Myocardial interstitial fibrosis. Results are expressed as mean ± SEM. n = 8 per group. $^{**}P < 0.01$.

treated cardiomyocytes. HG inhibited mitochondrial respiration potential in the cardiomyocytes, particularly maximum respiration and spare respiration, both of which were enhanced by BNP administration (Supplementary Figs. S4E and F). MitoSOX Red signals, marker of mitochondria-derived superoxide, was significantly increased in the cardiomyocytes exposed to HG. BNP administration reduced superoxide generation from mitochondria in the cardiomyocytes cultured in HG medium (Fig. 4A and B). BNP also inhibited the increase in the oxidation product of MitoSOX (2-OH-Mito-ethidium and Mito-ethidium) induced by high glucose (Fig. 4C–E). MitoTempo (mitochondria-targeted antioxidant, 25 nmol/L, MedChem Express) [28], Gp91ds-tat (a selective NOX2 inhibitor, 10 μmol/L, AnaSpec) [28], GKT137831 (a specific NOX4 inhibitor, 3 μmol/L, MedChem Express) [29], PEG-SOD (400 U/mL, Sigma-Aldrich) [30] and PEG-catalase (1000 U/mL, Sigma-Aldrich) [30] were used to identify the ROS sources under high glucose condition. Cardiomyocytes were incubated with high glucose for 24 h and then high glucose medium in the presence of the inhibitors for another 24 h. As shown in Fig. 4F–H, MitoTempo, Gp91ds-tat and PEG-SOD inhibited both cellular ROS and mitochondrial superoxide production induced by high glucose as determined by CM-H2DCFDA and MitoSOX Red staining, respectively. High glucose-induced cell apoptosis (as reflected via caspase 3 activity) was also inhibited by these three inhibitors (Fig. 4I). The results suggest that high glucose-induced oxidative stress mainly arises from mitochondria and NOX2 and can be scavenged by SOD. There is a potential interaction between mitochondrial and non-mitochondrial ROS. Afterwards, the role of decreased mitochondrial ROS in the BNP-mediated cardioprotection against DCM was further explored. Eight weeks after diagnosis, diabetic mice received daily injection of MitoTempo (0.7 mg/kg/day, i.p., MedChem Express) or vehicle for 4 weeks [28]. As shown in Fig. 4J-M, MitoTempo improved cardiac function and inhibited cell apoptosis in the diabetic hearts (Heart rate: Con 447.8 ± 8.81 bpm, DM 449.1 ± 10.17 bpm, DM + M-TEMPO 440.9±9.99 bpm, DM + M-TEMPO + BNP 445.9±10.39 bpm). A combination of MitoTempo and BNP did not provide further protection, suggesting the cardioprotection of BNP is mainly due to its antioxidant properties. These findings reveal that the BNP exerts direct protective action on the cardiomyocytes and mitochondria under HG condition.

The effects of BNP on mitochondrial biogenesis and dynamics were further analyzed. The primary cardiomyocytes cultured in NG medium showed elongated tubules, while the cardiomyocytes cultured in HG medium became spherical and shorter (Fig. 5A). The cardiomyocytes cultured with HG had reduced mitochondrial size and a higher number of mitochondria than NG-cultured cardiomyocytes. BNP treatment decreased the number of mitochondria per cell (Fig. 5B) and increased mean size of individual mitochondrion (Fig. 5C) in the HG-cultured cardiomyocytes, indicating that BNP promoted mitochondrial fusion under HG conditions. The relative content of mtDNA and mitochondrial mass were assessed by RT-qPCR and flow cytometry respectively to assess mitochondrial biogenesis. HG or BNP did not affect the mtDNA contents or mitochondrial mass (Fig. 5D–F), suggesting that HG or BNP did not stimulate mitochondrial biogenesis. Subsequently, mitochondrial fission/fusion-related protein expression profiles were examined. Western blot verified that Mfn1, Mfn2, Drp1 and Fis1 expression did not change between HG and NG treatment, only Opa1 expression was significantly reduced in HG-cultured cardiomyocytes. BNP administration increased Opa1 expression in HG-treated cardiomyocytes (Fig. 5G and H). RT-qPCR analysis revealed an increase in Opa1 mRNA levels after BNP administration in HG groups (Fig. 5I), suggesting that Opa1 expression appears to be primarily regulated at the transcriptional level (mRNA level). Together, these data indicated that BNP elevated Opa1 transcription and mitochondrial fusion as well as mitochondrial function under hyperglycemic condition *in vivo* and *in vitro*.

3.4. Knockdown of BNP impaired cardiac function and inhibited Opa1-mediated mitochondrial fusion

To further investigate the role of BNP in the development of DCM, adeno-associated virus expressing BNP shRNA (AAV-BNP shRNA) were used to knock down BNP in the myocardium *in vivo*. Fig. 6A–B shown

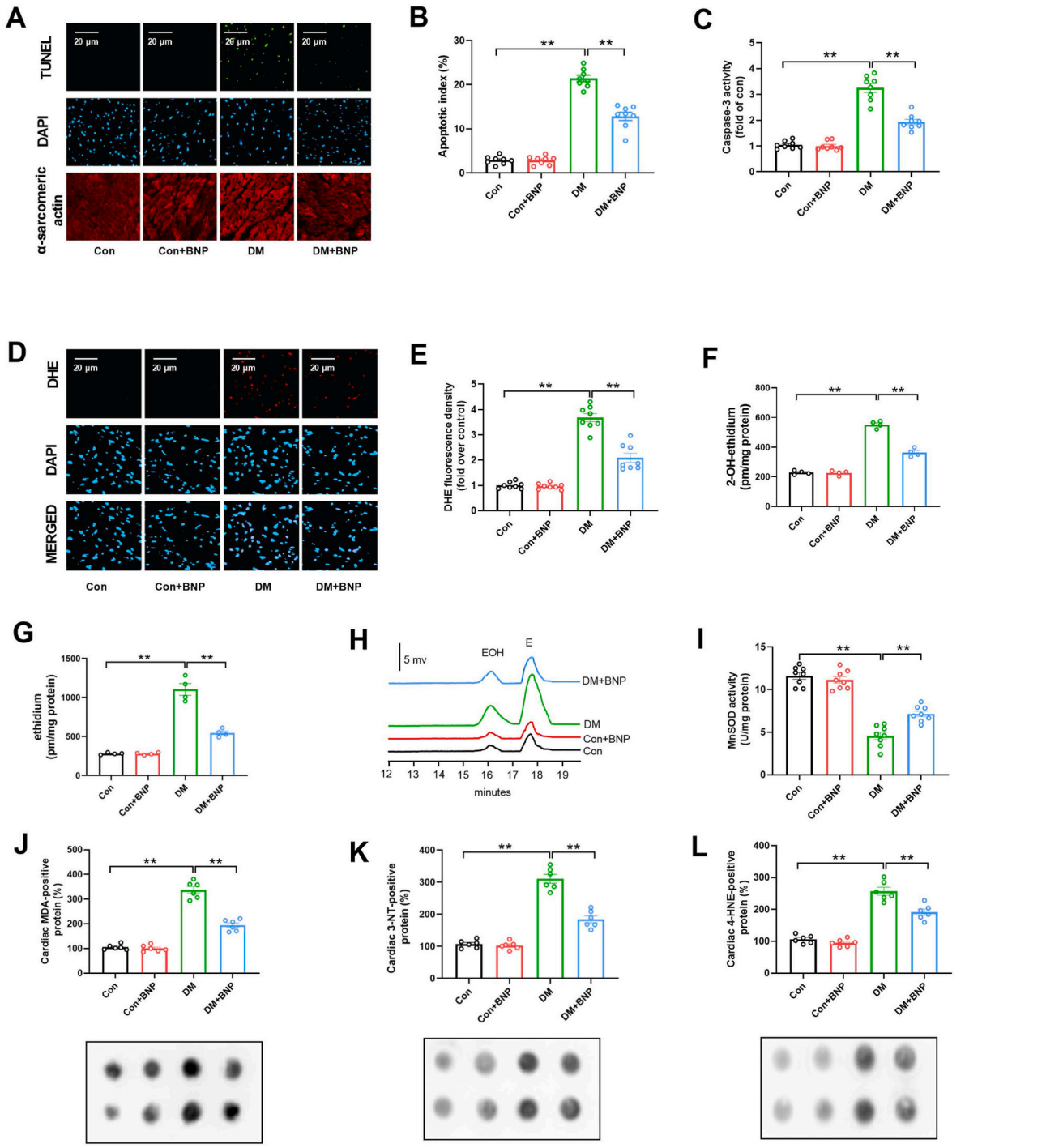

Fig. 2. BNP treatment significantly decreased the apoptosis and oxidative stress in the diabetic hearts. (A) Representative image of TUNEL-positive cells (green) and DAPI (blue) in heart sections. Scale bars = 20 μm. (B) Apoptotic index: percentage of TUNEL-positives apoptotic cells. (C) Myocardial caspase-3 activity (fold over Con). (D) Representative images of DHE (red) and DAPI (blue) staining in heart sections. (E) Quantification of DHE fluorescence (fold over Con). (F–H) EOH (2-OH-ethidium) and E (ethidium) obtained by HPLC analysis. (I) The activity of MnSOD. (J) Malondialdehyde (MDA). (K) 3-nitrotyrosine (3-NT). (L) 4-hydroxynonenal (4-HNE). Results are expressed as mean ± SEM. n = 4–8 per group. $^{**}P < 0.01$. (For interpretation of the references to colour in this figure legend, the reader is referred to the Web version of this article.)

that AAV-BNP shRNA significantly decreased BNP protein expression in the hearts of diabetic mice. Plasma BNP concentrations were also decreased by AAV-BNP shRNA in the diabetic mice (Fig. 6C). Echocardiography analysis showed that knockdown of BNP decreased LVEF and LVFS in the control hearts and further exacerbated cardiac dysfunction in diabetic mice (Fig. 6D–F) (Heart rate: Con + AAV-Con shRNA 445.4 ±9.48 bpm, DM + AAV-Con shRNA 448.4±11.47 bpm, Con + AAV-BNP shRNA 444.5±6.65 bpm, DM + AAV-BNP shRNA 453.3±12.80 bpm). Additionally, BNP knockdown worsened myocardial apoptosis and oxidative stress in diabetic hearts (Fig. 6G-L).

The impact of BNP knockdown on mitochondrial dynamics was then explored *in vitro*. Small interfering RNA (RNAi) was used to knockdown BNP in both NG or HG-treated cardiomyocytes. In Fig. 7A–F, silencing BNP expression with RNAi inhibited Opa1 expression and mitochondrial

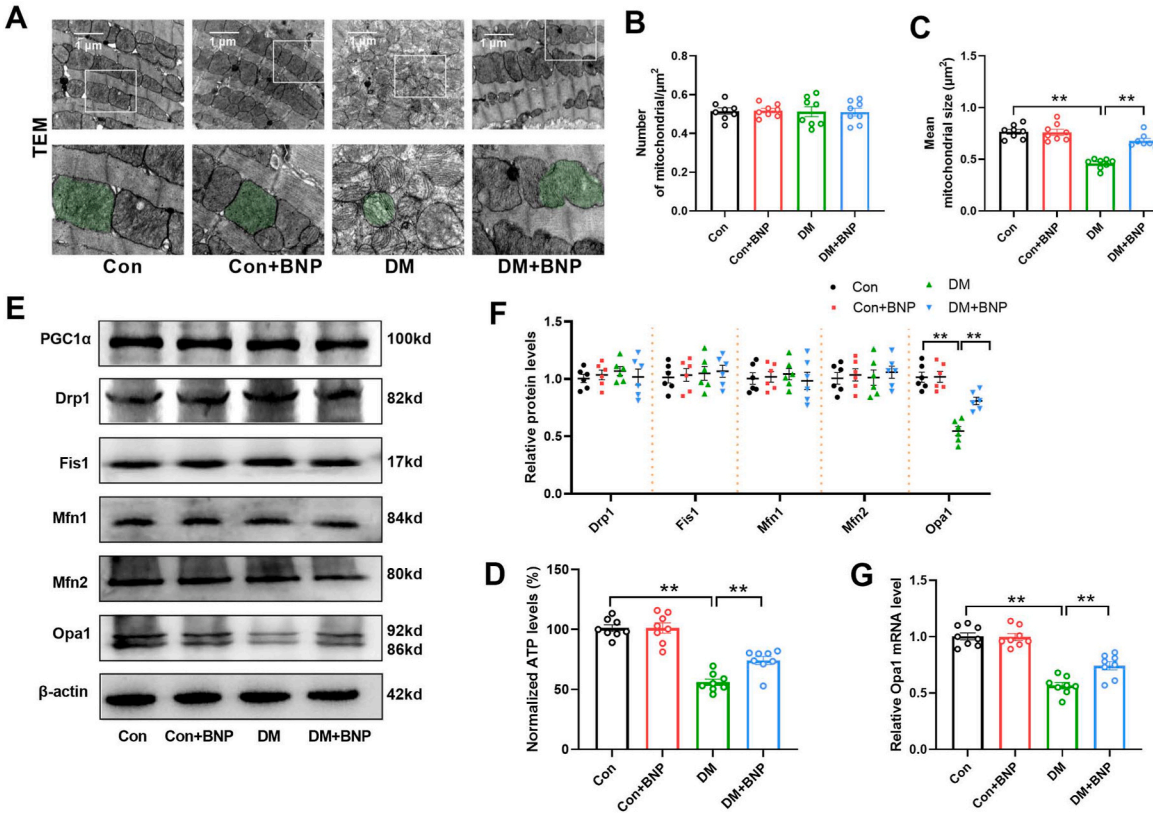

Fig. 3. BNP treatment enhanced Opa1-mediated mitochondrial fusion in diabetic hearts. (A) Representative transmission electron microscopy images (TEM) of the myocardium. Mitochondria are shown in green. Scale bars are 1 mm. (B) The number of mitochondria per um. (C) Mean mitochondrial size. (D) A normalized level of ATP. (E) Representative blot images of mitochondrial fission and fusion-associated proteins (Mfn1, Mfn2, Opa1, Drp1 and Fis1). (F) Protein expressions are quantitatively analyzed. (G) Expression of Opa1 mRNA is quantitatively analyzed. Results are expressed as mean ± SEM. n = 6–8 per group. $^{**}P < 0.01$. (For interpretation of the references to colour in this figure legend, the reader is referred to the Web version of this article.)

fusion in the cardiomyocytes cultured in NG medium. Moreover, BNP knockdown further suppressed mitochondrial fusion and Opa1 expresssion under HG condition (Fig. 7A–F). In addition, BNP RNAi increased mitochondrial oxidative stress/celluar apoptosis (Fig. 7D, G-I) and impaired mitochondrial membrane potential/mitochondrial respiratory capacity (Fig. 7J-M) in both NG or HG-treated cardiomyocytes. Taken together, these results indicate that BNP knockdown exacerbated myocardial oxidative stress/apoptosis and suppressed Opa1-mediated mitochondrial fusion under diabetic condition.

3.5. *Opa1 knockdown blunted the beneficial effects of BNP under diabetic condition*

Next, we went on to investigate whether increased Opa1 expression was essential for the protective action of BNP on the diabetic hearts and mitochondria. In Supplementary Fig. S5, Opa1 RNAi blunted BNP's stimulating effects on mitochondrial fusion while eliminating BNP's inhibitory effects on mitochondrial oxidative stress as well as apoptosis in HG-treated cardiomyocytes. Then, cardiac-specific Opa1 knockdown mice were generated by using AAV-Opa1 shRNA. As shown in Fig. 8A and B, the expression of Opa1 protein was significantly decreased by AAV-Opa1 shRNA in the diabetic heart. Opa1 knockdown blunted the promoting effects of BNP on cardiac function (Fig. 8C–E) and mitochondrial fusion (Fig. 8F–H). (Heart rate: DM + AAV-Con shRNA 452.6.4±9.99 bpm, DM + BNP + AAV-Con shRNA 447.5±11.38 bpm, DM + AAV-Opa1 shRNA 451.9±10.99 bpm, DM + BNP + AAV-Opa1 shRNA 449.8±12.86 bpm). Moreover, BNP's inhibitory effects on apoptosis (Fig. 8I–K) and oxidative stress (Fig. 8L-N) were blocked in the diabetic hearts when Opa1 was knocked down. The data suggested that BNP promoted mitochondrial fusion and provided cardiac protection in an Opa1-dependent manner.

3.6. *BNP elevated Opa1 expression via STAT3-iduced transcription*

We next sought to explore how BNP upregulated the Opa1 expression. Several specific inhibitors including pyrrolidine dithiocarbamate (PDTC, an NF-κB inhibitor, 100 μmol/L) [31], wortmannin (Wort, a PI3K/Akt inhibitor, 0.1 μmol/L, MedChem Express) [32,33], PD98059 (a MEK/ERK inhibitor, 20 μmol/L, MedChem Express) [34,35], bisindolylmaleimide I (Bis, a PKC inhibitor, 10 μmol/L, MedChem Express) [36,37], and Stattic (a STAT3 inhibitor, 10 μmol/L, MedChem Express) [38,39] were used to block the activation of signaling pathways in the cardiomyocytes. BNP-induced elevation of Opa1 was largely abolished by STAT3 inhibitor but not the other inhibitors (Fig. 9A and B), suggesting that BNP-induced elevation of Opa1 expression is mediated by STAT3 signaling pathways. As expected, BNP treatment significantly reversed the decrease in phosphorylated STAT3 (p-STAT3) protein expression in the HG-treated cardiomyocytes (Supplementary Fig. S6). The role of STAT3 was further confirmed by the siRNA. STAT3 RNAi not only blunted BNP's promoting effects on Opa1-mediated mitochondrial fusion (Fig. 9C–I), but also blocked BNP's inhibition on mitochondrial oxidative stress (Fig. 9G and J) and apoptosis (Fig. 9K and L) in the HG-treated cardiomyocytes. Moreover, STAT3 was found to be directly bound to the promoter of Opa1. There was decreased binding of STAT3 to the Opa1 promoter in HG-cultured cardiomyocytes. BNP treatment significantly restored this binding (Fig. 9M). The results indicate that the promoting effects of BNP on Opa1-mediated mitochondrial fusion is dependent on the STAT3-mediated transcriptional manner.

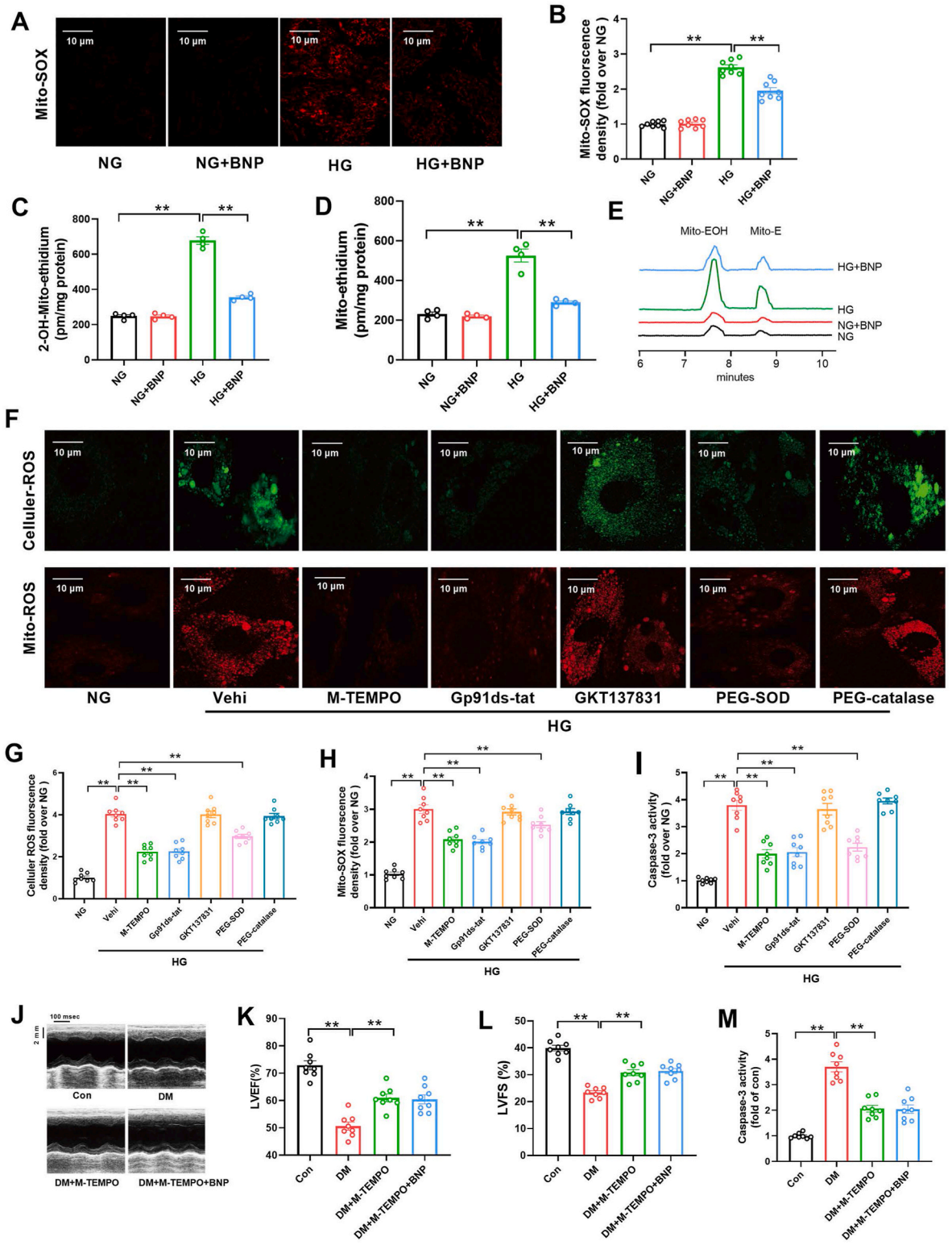

Fig. 4. BNP protected against mitochondrial oxidative stress and apoptosis. (A) Representative confocal fluorescent images of mitochondrial superoxide production detected by MitoSOX. Original magnification × 600. (B) Quantification of MitoSOX fluorescence density (fold over NG). (C–E) 2-OH-Mito-ethidium and Mito-ethidium, the superoxide-specific product of MitoSOX, was measured using HPLC analysis. (F) Representative images of cellular ROS production (green fluorescence) and MitoSOX-stained mitochondrial ROS (red fluorescence). Original magnification × 600. (G) Quantitative data of relative whole-cell ROS fluorescence density expressed as a fold change compared with NG. (H) Quantitative data of relative mitochondrial ROS fluorescence density expressed as a fold change compared with NG. (I) Activity of myocardial caspase-3 (fold over NG). (J) Representative M-mode echocardiography images. (K) Left ventricular ejection fraction (LVEF). (L) Left ventricular fractional shortening (LVFS). (M) Activity of myocardial caspase-3 (fold over Con). n = 4–8. Data are shown as mean ± SEM. $^{**}P < 0.01$. (For interpretation of the references to colour in this figure legend, the reader is referred to the Web version of this article.)

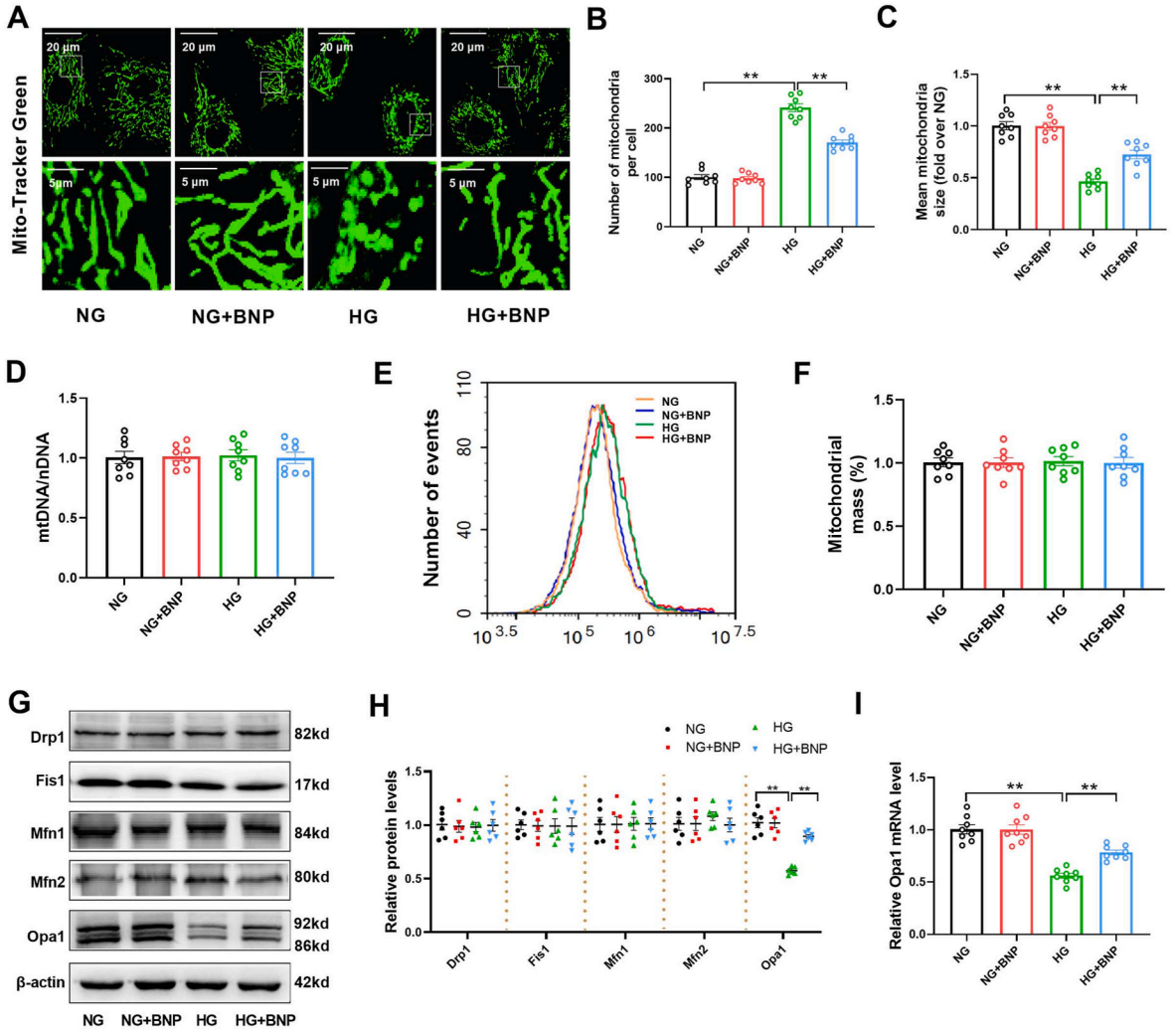

Fig. 5. BNP promoted mitochondrial fusion and enhanced mitochondrial respiratory capacity in high glucose (HG)-cultured cardiomyocytes. (A) Representative images of mitochondrial morphology stained with MitoTracker Green, original magnification: 600 × . (B) Averaged mitochondrial number per cell. (C) Mean mitochondrial size (fold over NG). (D) RT-qPCR was performed to quantify the ratio of mtDNA relative to nuclear DNA (mtDNA/nDNA). (E) Flow cytometry was carried out to assess the mitochondria mass using the MitoTracker Green staining. (F) Quantitative analysis of mitochondria mass. (G, H) Representative blot images and quantitative analysis of mitochondrial fission proteins and fusion proteins. (I) Quantitative expression of Opa1 mRNA. Results are expressed as mean ± SEM. n = 6–8 per group. $^{**}P < 0.01$. (For interpretation of the references to colour in this figure legend, the reader is referred to the Web version of this article.)

3.7. BNP activated STAT3-Opa1 signaling pathway via stimulating NPRA-PKG

BNP binds to its receptor NPRA and then activates the PKG signaling to exert the biological function [40,41]. The expression and activity of PKG were then measured in the cardiomocytes. As shown in Fig. 10A–B, there was no significant changes in PKG expression among all the groups. HG induced a decrease in PKG activity. BNP significantly increased PKG activity in both NG or HG-cultured cardiomyocytes (Fig. 10C). PKG or NPRA siRNA was further used to explore the role of NPRA-PKG signaling in the protective effects of BNP. It was shown that PKG or NPRA RNAi not only inhibited the upregulating effects of BNP on PKG activity and STAT3 phosphorylation (Fig. 10D–F) as well as Opa1-mediated mitochondrial fusion (Fig. 10G–I), but also greatly abrogated the inhibitory effects of BNP on mitochondrial oxidative stress (Fig. 10G and J) and cellular apoptosis (Fig. 10K and L) under HG condition. Co-immunoprecipitation experiments indicated that STAT3 was precipitated with PKG antibody, suggesting that PKG may interact with STAT3 directly and induce STAT3 activation through phosphorylation. The interaction was dramatically reduced under HG conditions. BNP treatment restored the interaction of STAT3 with PKG in cardiomyocytes treated with HG (Fig. 10M and N). The data suggested that PKG might act as a critical molecule of BNP signaling to activate STAT3-Opa1 pathway and promote mitochondrial fusion.

4. Discussion

The initial aim of this study is to explore the role of BNP in the development of diabetic cardiomyopathy (DCM). It is an interesting translational research since heart failure is often accompanied by increased serum BNP levels in clinical observation. Moreover, BNP has been used in the clinical treatment of patients with heart failure. We have found that increased plasma BNP level precedes the occurrence of DCM. BNP administration preserves mitochondrial function and prevented the development of DCM, while BNP knockdown impaired mitochondrial function and aggravated cardiac dysfunction. This study reveals that there is an increased level of BNP at the early stage of DCM as a compensatory protection (Fig. 11). Given the availability of BNP detection and application in clinical practice, our study possesses important translational implications that BNP could be used for the early diagnosis and treatment of DCM.

In terms of mechanism, we have considered two aspects on the

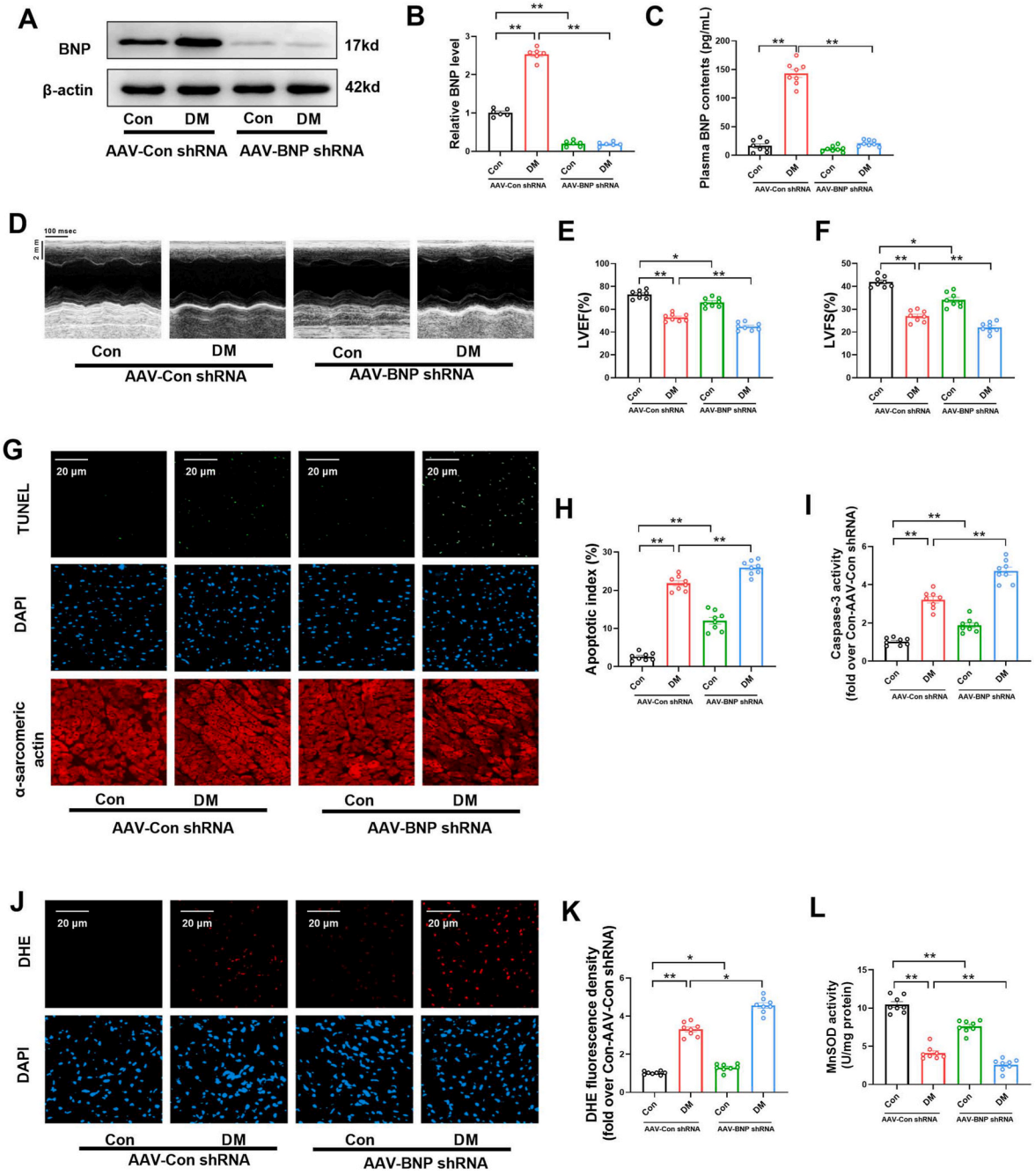

Fig. 6. BNP knockdown exacerbated cardiac dysfunction, myocardial apoptosis and oxidative stress in the diabetic hearts. (A, B) Representative blots and quantitative analysis of BNP. (C) Plasma BNP contents. (D) Representative echocardiography images. (E, F) Quantitative evaluation of LVEF and LVFS. (G) Representative image of TUNEL-positive cells (green) and DAPI (blue) in heart sections. Scale bars = 20 μm. (H) Apoptotic index: percentage of TUNEL-positives apoptotic cells. (I) Activity of myocardial caspase-3 (fold over Con-AAV-Con shRNA). (J) Representative images of DHE (red) and DAPI (blue) staining in heart sections. (K) Quantification of DHE fluorescence (fold over Con-AAV-Con shRNA). (L) MnSOD activity. Results are expressed as mean ± SEM. n = 6–8 per group. $^{*}P < 0.05$, $^{**}P < 0.01$. (For interpretation of the references to colour in this figure legend, the reader is referred to the Web version of this article.)

regulation of mitochondrial function including mitochondrial biogenesis and mitochondrial fusion/fission dynamics. It was found that BNP did not affect mitochondrial biogenesis while promoted mitochondrial fusion. BNP binds to its receptor NPRA and activates PKG that consequently interacts with STAT3, which phosphorylates and activates STAT3-Opa1 signaling and then inhibits mitochondrial ROS (Fig. 11). Compared with exogenous compounds such as punicalagin or paeonol in the previous studies [26,42], BNP is an endogenous bioactive substance produced inside the body. One novelty of our current study is that we have identified an endogenous bioactive substance BNP as a new mitochondrial fusion promoter to protect against DCM, suggesting that endogenous bioactive substances have regulatory function for the balance of mitochondrial fusion/fission dynamics. The balance can be broken in the event of endocrine disorder.

The coordination of both the outer and inner membranes is involved in the process of mitochondria fusion. Mfn1 and Mfn2 are required for the fusion of the outer mitochondrial membrane, and Opa1 is essential for mitochondrial inner membrane fusion [43]. In the present study, only Opa1 expression was significantly reduced in diabetic hearts, whereas the expression of other mitochondrial fusion proteins including

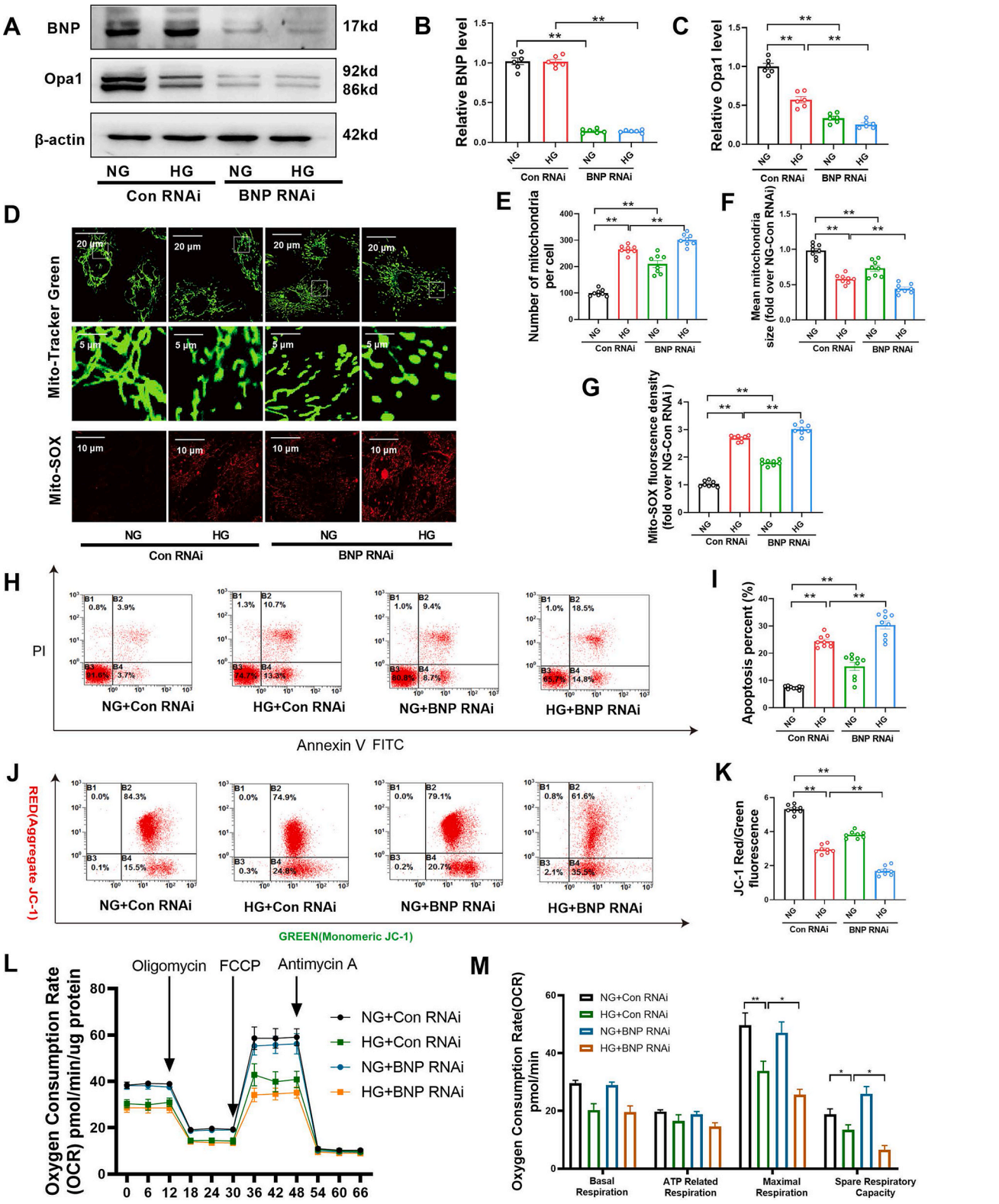

Fig. 7. BNP knockdown induced oxidative stress/apoptosis and suppressed Opa1-mediated mitochondrial fusion in both NG or HG-treated cardiomyocytes. (A–C) Representative blot images and quantitative analysis of BNP and Opa1. (D) Confocal images of mitochondrial morphology stained with MitoTracker Green (upper) and mitochondrial ROS stained with MitoSOX Red (below). (E) Averaged mitochondrial number per cell. (F) Mean mitochondrial size (fold over NG-Con RNAi) (G) Quantitative analysis of MitoSOX Red fluorescence density (fold over NG-Con RNAi). (H) JC-1 staining was used to determine mitochondrial membrane potential by flow cytometry. (I) Mitochondrial membrane potential was quantified. (J) An Annexin V-FITC/PI labeling was used to determine cellular apoptosis by flow cytometry. (K) Percentage of apoptotic cell populations. (L) Oxygen consumption rates (OCR) was measured by an XF24 analyzer. (M) Quantitative analysis of OCR. Results are expressed as mean ± SEM. n = 6–8 per group. $^{*}P < 0.05$, $^{**}P < 0.01$. (For interpretation of the references to colour in this figure legend, the reader is referred to the Web version of this article.)

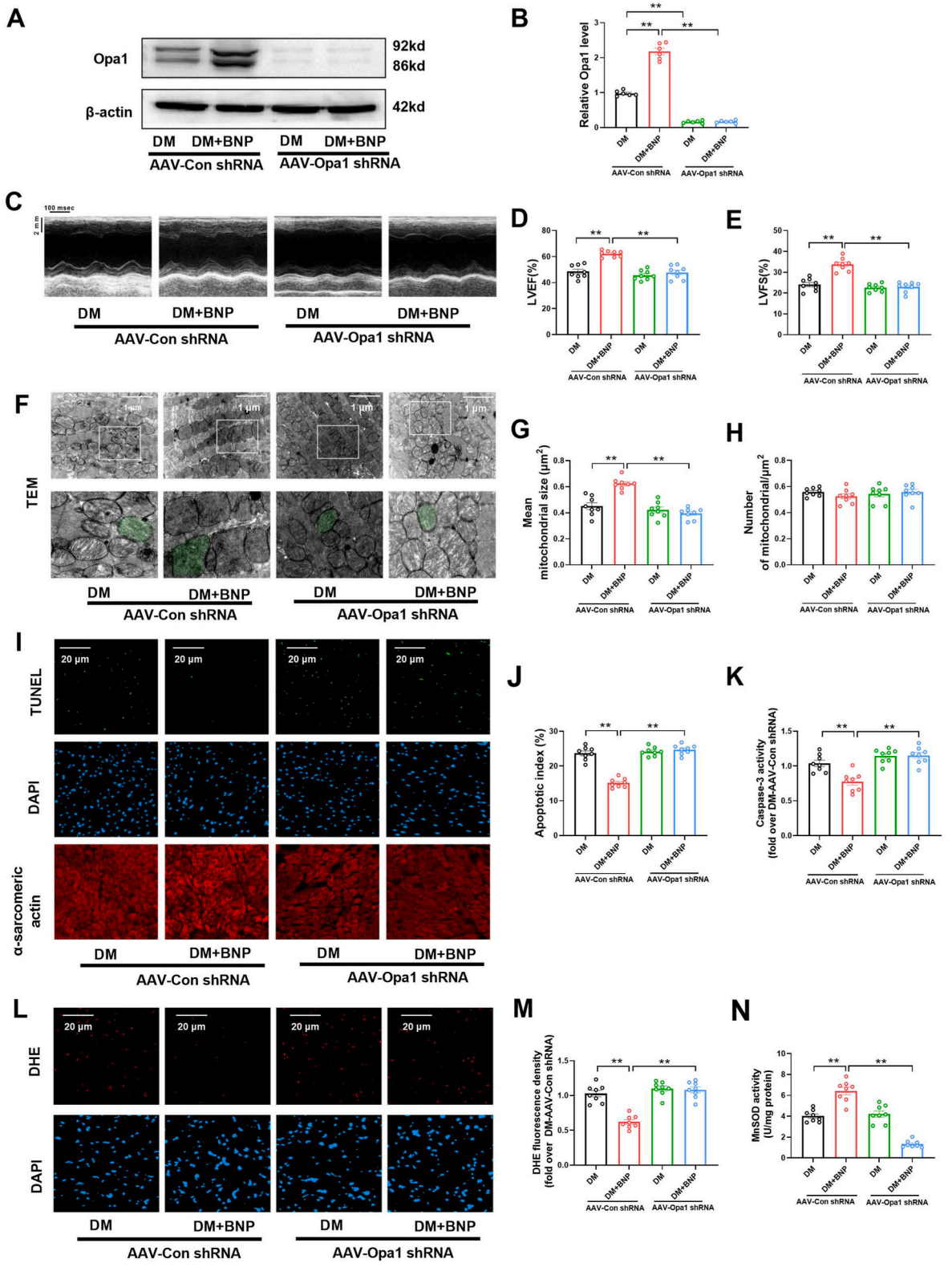

Fig. 8. Opa1 knockdown blunted the protective effects of BNP on mitochondrial fusion in diabetic mice. (A, B) Representative blot images and quantitative analysis of Opa1 treated with AAV-Opa1 shRNA or AAV-Con shRNA. (C) Representative M-mode echocardiography images. (D, E) Left ventricular ejection fraction (LVEF) and Left ventricular fractional shortening (LVFS). (F) Representative transmission electron microscopy images (TEM) of the myocardium. Mitochondria are shown in green. Scale bars are 1 mm. (G) Mean mitochondrial size. (H) The number of mitochondria per um. (I) Representative image of TUNEL-positive cells (green) and DAPI (blue) in heart sections. Scale bars = 20 μm. (J) Apoptotic index: percentage of TUNEL-positives apoptotic cells. (K) Activity of myocardial caspase-3 (fold over DM-AAV-Con shRNA). (L) Representative images of DHE staining (red) and DAPI (blue) in heart sections. (M) Quantification of DHE fluorescence (fold over DM-AAV-Con shRNA). (N) MnSOD activity. Results are expressed as mean ± SEM. n = 6–8 per group. $^{**}P < 0.01$. (For interpretation of the references to colour in this figure legend, the reader is referred to the Web version of this article.)

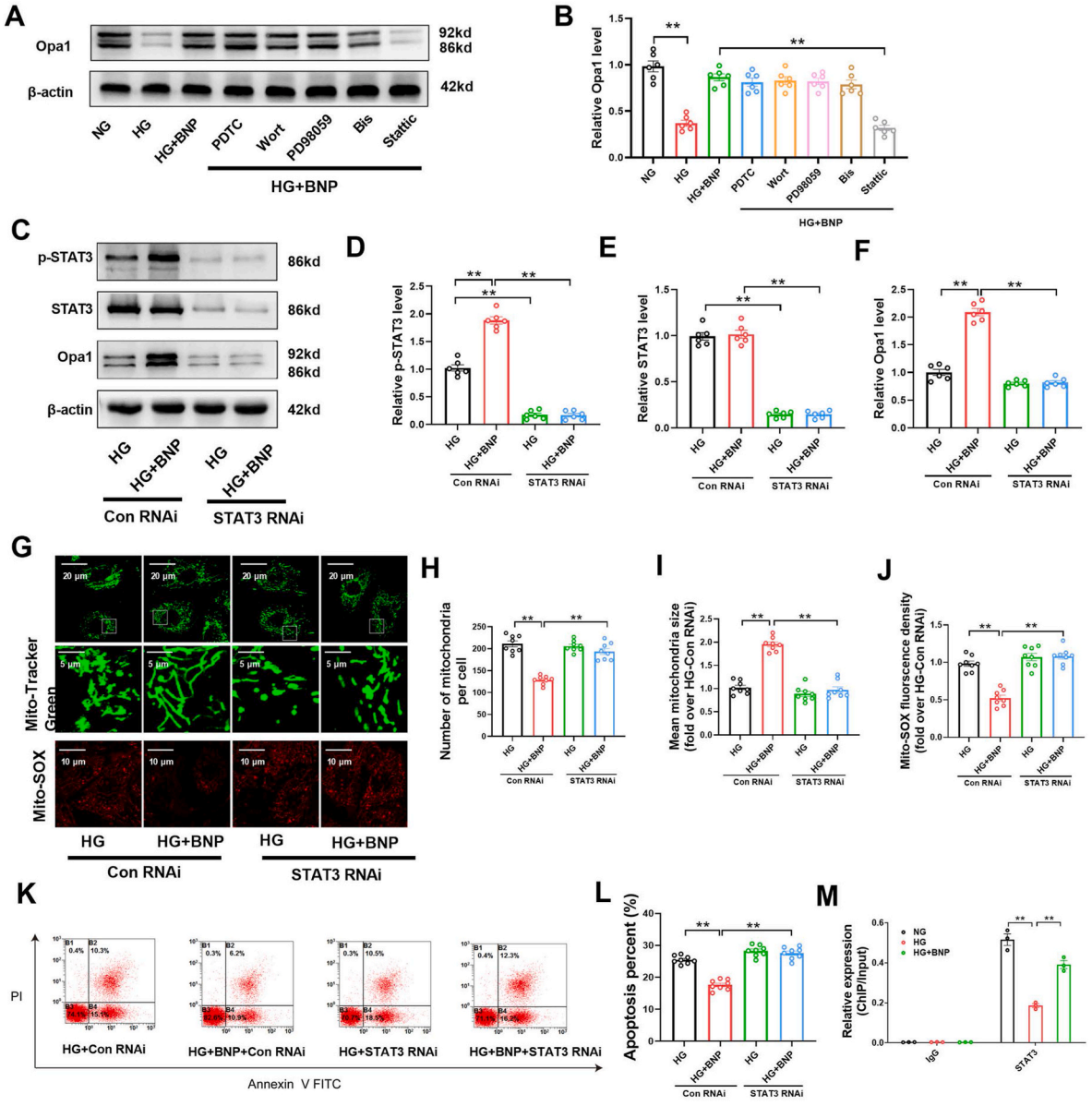

Fig. 9. STAT3 signaling was essential for BNP-induced Opa1 upregulation in HG-treated cardiomyocytes. (A) The cells were treated with several inhibitors of signaling cascades, which include dithiocarbamate (PDTC, NF-kB inhibitor), wortmannin (Wort, PI3K inhibitor), PD98059 (MEK/ERK inhibitor), bisindolylmaleimide I (Bis I, PKC inhibitor), and stattic (STAT3 inhibitor). (B) Opa1 expression levels were quantified. (C–F) Representative blot images and quantitative analysis of p-STAT3, STAT3, and Opa1. (G) Confocal images of mitochondrial morphology stained with MitoTracker Green (upper) and mitochondrial ROS stained with MitoSOX Red (below). (H) Averaged mitochondrial number per cell. (I) Mean size of mitochondria (fold over HG-Con RNAi). (J) Quantitative analysis of MitoSOX Red fluorescence density (fold over HG-Con RNAi). (K) An Annexin V-FITC/PI labeling was used to determine cellular apoptosis by flow cytometry. (L) Percentage of apoptotic cell populations. (M) ChIP assay investigated the binding of STAT3 to the Opa1 promoter. Results are expressed as mean ± SEM. n = 3–8 per group. $^{**}P < 0.01$. (For interpretation of the references to colour in this figure legend, the reader is referred to the Web version of this article.)

Mfn1 and Mfn2 was unaltered. This might be partly attributed to insulin deficit in the STZ-induced diabetic models, as insulin is demonstrated to upregulate Opa-1 in the cardiomyocytes without impacting Mfn1 and Mfn2 expression [44]. Long forms (L-Opa1) and short forms Opa1 (S-Opa1) can be synthesized by proteolytic cleavage. Song et al. have found that both L-Opa1 and S-Opa1 are necessary for mitochondrial fusion [45]. Our work reveals that Opa1 may not be proteolytically cleaved by hyperglycemia or BNP administration, since long and short forms of Opa1 were not selectively affected by high glucose or BNP. ROS are mainly produced by mitochondria in the electron transport chain (ETC), which lies inside the inner mitochondrial membrane. Opa1-mediated mitochondrial fusion could affect the inner mitochondrial membrane and ETC components assembly, thereby inhibiting ROS production and enhancing ETC activity. In addition, mitochondrial fusion has the potential to alter the spatial and structural organization of ATP synthase [46]. An increase in the activities of ETC and ATP synthase then leads to an increase in ATP production. In addition, Opa1 is a modulator of mitochondrial cristae shape, a mechanism that enhances electron transport and increases mitochondrial respiration capacity [47,48]. Therefore, Opa1 protects against DCM not only via promoting mitochondrial fusion but may also via cristae remodeling.

BNP has been shown to protect mitochondria in previous studies [49,50], while the direct link between the mitochondria and BNP signaling pathway is still largely unknown. BNP induces cellular responses through its receptor NPRA and the activation of PKG, which exerts its biological functions by phosphorylating target proteins [51,52]. PKG is

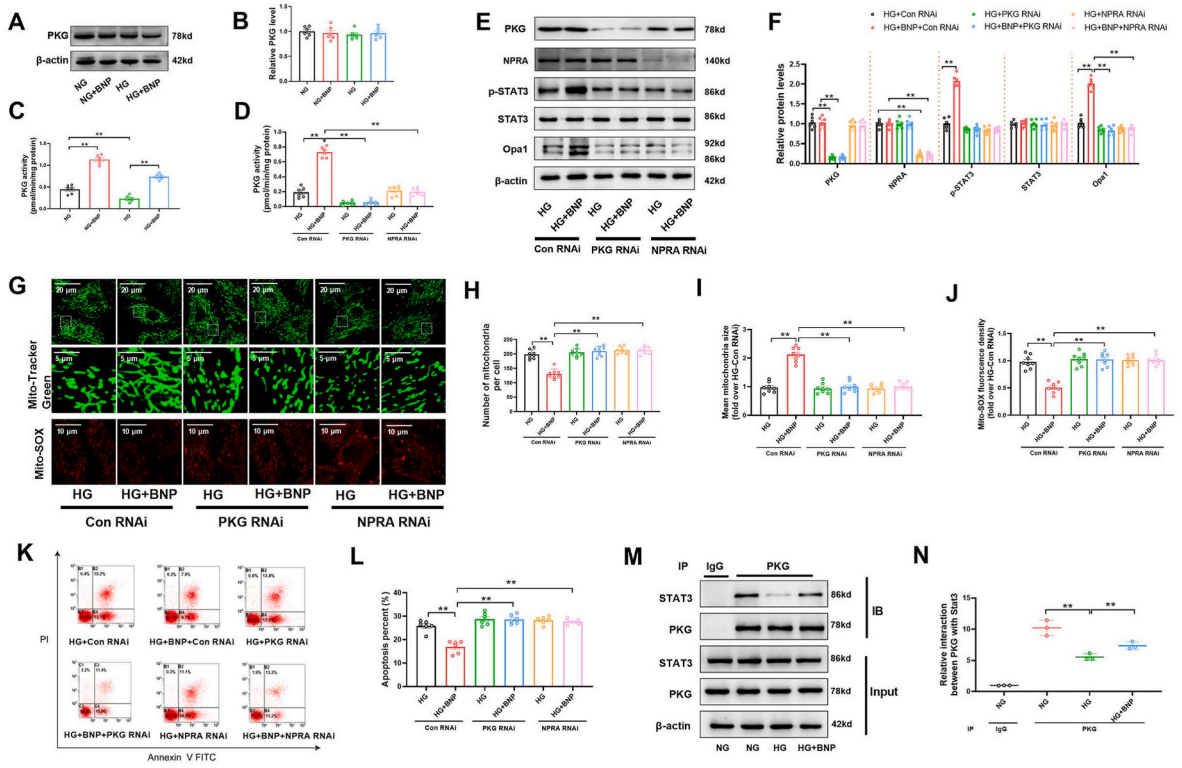

Fig. 10. PKG was essential for BNP-induced activation of STAT3-Opa1 signaling pathway in HG-treated cardiomyocytes. (A–B) Representative blot images and quantitative analysis of PKG. (C–D) PKG activity. (E–F) Representative blot images and quantitative analysis of PKG, NPRA, p-STAT3, STAT3, and Opa1. (G) Confocal images of mitochondrial morphology stained with MitoTracker Green (upper) and mitochondrial ROS stained with MitoSOX Red (below). (H) Averaged mitochondrial number per cell. (I) Mean size of mitochondria (fold over HG-Con RNAi). (J) Quantitative analysis of MitoSOX Red fluorescence density (fold over HG-Con RNAi). (K) An Annexin V-FITC/PI labeling was used to determine cellular apoptosis by flow cytometry. (L) Quantification of apoptotic cells. (M − N) Co-IP revealed PKG-STAT3 interaction. Results are expressed as mean ± SEM. n = 3–8 per group. $^{**}P < 0.01$. (For interpretation of the references to colour in this figure legend, the reader is referred to the Web version of this article.)

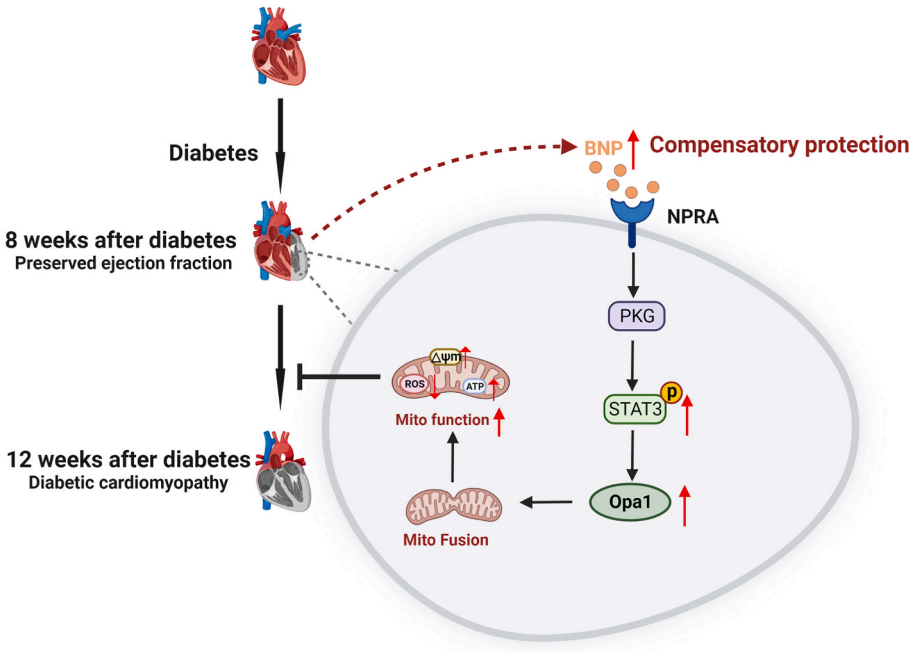

Fig. 11. Schematic figure showing that there is an increased level of BNP at the early stage of diabetic cardiomyopathy as a compensatory protection. BNP binds to its receptor NPRA and activates PKG that consequently interacts with STAT3, which phosphorylates and activates STAT3-Opa1 signaling and then enhances mitochondrial fusion. Subsequently, BNP-induced mitochondrial fusion inhibits mitochondrial dysfunction and mitigates diabetic cardiomyopathy. Mito, mitochondrial; ROS, reactive oxygen species; △Ψm, mitochondrial membrane potential.

considered as a common mediator of cardioprotection [53]. Enhanced PKG signaling was accompanied with reduced cardiomyocyte hypertrophy, inhibited fibrotic remodeling, and significantly improved cardiac performance in diabetic hearts [54]. The PKG-mediated inhibition of mitochondrial permeability transition and cytochrome *c* production performs a crucial function in ischemic heart disease [55]. In

addition, PKG-dependent signaling reduces myocardial apoptosis and oxidative stress and preserves cardiac function in diabetic myocardial ischemia-reperfusion injury [56]. Here, an important observation is that we have shown that PKG interacts with STAT3 directly and induces STAT3 activation and then promotes the transcription of Opa1. This result sheds light on the detailed downstream mechanisms of how BNP promotes Opa1-mediated mitochondrial fusion. Notably, BNP does not affect the expression of Opa1 in non-diabetic conditions. This is possibly due to the level of STAT3 phosphorylation is already relatively high and activation of BNP-PKG signaling will exert little additional effect.

Eric and colleagues have shown that plasma BNP concentration is increased in the diabetic db/db mice [11]. Cardiac BNP expression is also reported to be increased in diabetic animals [57,58]. Consistent with previous studies, we found that STZ-induced diabetic animals have an enhanced expression of cardiac BNP and a higher plasma BNP level *in vivo*. BNP is significantly increased in diabetic patients with cardiac dysfunction, but it does not correlate with diabetic severity. This may be due to the fact that BNP is secreted after the heart is stretched, while BNP secretion is not directly stimulated by hyperglycemia. Our results have shown that high glucose does not change the expression of BNP in the cardiomycytes *in vitro* (Fig. 7A). It seems that the production of increased BNP in DCM is due to the response of ventricle to stretch but not high glucose [59]. BNP is generally considered to cause a reduction in blood pressure [60]. In our investigation, no significant difference in blood pressure was detected in control or diabetic mice following BNP administration, presumably because BNP was delivered at a low dosage (0.75 μg/kg/h, dose equivalent to 18 μg/kg/d) via minipump infusion. Similar results were also reported in a previous study in which blood pressure was not significantly changed when BNP was injected every 2 days at the dose of 2 μg/mouse (equivalent to 50 μg/kg/d) [61]. Moreover, NPRA protein levels are gradually reduced during the process of DCM, which are associated with increased serum BNP levels. These observations suggest that BNP resistance may be developed in diabetic hearts. It needs to note that early treatment is important for BNP to exert its cardioprotective effects in DCM, since the protection of late BNP treatment might be largely blunted by BNP resistance at late stage of DCM. In that case, a much greater dose of BNP may be required to induce the similar effects of early treatment. This issue needs to be explored in further study. In addition, it appears that early BNP treatment promotes moderate improvement in fibrosis, but is accompanied with a rather modest improvement in LVEF. We expect that there to be continued improvement in cardiac function with a longer course of BNP treatment.

This research still has some limitations. First, it is crucial to note that Opa1 might not be the exclusive critical molecule implicated in BNP's cardioprotective activities, since a multitude of signaling pathways might be involved in the cardioprotective effects of BNP. Second, NPRA-PKG-STAT3 signaling was mainly explored *in vitro* using siRNA. Knockdown of NPRA, PKG or STAT3 in the hearts *in vivo* could provide more solid evidences to support the conclusion. Third, despite the fact that STZ-induced mice have been employed as the experimental diabetes model in a number of investigations [15,62], this model cannot perfectly mimic clinical diabetes in humans. Additional research may be required to elucidate the role of BNP in other types of DCM. Despite these limitations, we consider that our findings offer novel and significant understanding into the role of BNP in DCM.

It is concluded that there is an increased level of BNP at the early stage of DCM as a compensatory protection mechanism. BNP could protect against hyperglycemia-induced mitochondrial oxidative injury and DCM by upregulating Opa1 expression, a process in which BNP binds to its receptor NPRA and activates PKG that subsequently increasing STAT3 phosphorylation and enhancing Opa1 transcription. These findings suggest that BNP is a potential mitochondrial fusion promoter for preventing diabetes-related cardiac disorders.

Funding

This work was supported by the National Natural Science Foundation of China (No. 81870172, 82070387), and the grant from Shaanxi Provincial Key Research and Development Project (No. 2023JCZD55, 2022KWZ-18 and 2021JQ787).

Declaration of competing interest

The authors declare no conflict of interest.

Data availability

Data will be made available on request.

Appendix A. Supplementary data

Supplementary data to this article can be found online at https://doi.org/10.1016/j.redox.2023.102702.

References

[1] N.H. Cho, J.E. Shaw, S. Karuranga, Y. Huang, J.D. da Rocha Fernandes, A. W. Ohlrogge, B. Malanda, IDF Diabetes Atlas: global estimates of diabetes prevalence for 2017 and projections for 2045, Diabetes Res. Clin. Pract. 138 (2018) 271–281.
[2] S.E. Engelen, Y. van der Graaf, M.C. Stam-Slob, D.E. Grobbee, M.J. Cramer, L. J. Kappelle, G.J. de Borst, F.L.J. Visseren, J. Westerink, S.s. group, Incidence of cardiovascular events and vascular interventions in patients with type 2 diabetes, Int. J. Cardiol. 248 (2017) 301–307.
[3] S. Boudina, E.D. Abel, Diabetic cardiomyopathy revisited, Circulation 115 (25) (2007) 3213–3223.
[4] J.G. He, Y.L. Chen, B.L. Chen, Y.Y. Huang, F.J. Yao, S.L. Chen, Y.G. Dong, B-type natriuretic peptide attenuates cardiac hypertrophy via the transforming growth factor-ss1/smad7 pathway in vivo and in vitro, Clin. Exp. Pharmacol. Physiol. 37 (3) (2010) 283–289.
[5] Y. Chen, F. Yao, S. Chen, H. Huang, L. Wu, J. He, Y. Dong, Endogenous BNP attenuates cardiomyocyte hypertrophy induced by Ang II via p38 MAPK/Smad signaling, Pharmazie 69 (11) (2014) 833–837.
[6] A.M. Moilanen, J. Rysa, E. Mustonen, R. Serpi, J. Aro, H. Tokola, H. Leskinen, A. Manninen, J. Levijoki, O. Vuolteenaho, H. Ruskoaho, Intramyocardial BNP gene delivery improves cardiac function through distinct context-dependent mechanisms, Circ Heart Fail 4 (4) (2011) 483–495.
[7] G. Hu, X. Huang, K. Zhang, H. Jiang, X. Hu, Anti-inflammatory effect of B-type natriuretic peptide postconditioning during myocardial ischemia-reperfusion: involvement of PI3K/Akt signaling pathway, Inflammation 37 (5) (2014) 1669–1674.
[8] V.I. Publication, Committee for the, Intravenous nesiritide vs nitroglycerin for treatment of decompensated congestive heart failure: a randomized controlled trial, JAMA 287 (12) (2002) 1531–1540.
[9] W.J. Fang, C.J. Wang, Y. He, Y.L. Zhou, X.D. Peng, S.K. Liu, Resveratrol alleviates diabetic cardiomyopathy in rats by improving mitochondrial function through PGC-1alpha deacetylation, Acta Pharmacol. Sin. 39 (1) (2018) 59–73.
[10] R.H. Ritchie, J.E. Love, K. Huynh, B.C. Bernardo, D.C. Henstridge, H. Kiriazis, Y. K. Tham, G. Sapra, C. Qin, N. Cemerlang, E.J. Boey, K. Jandeleit-Dahm, X.J. Du, J. R. McMullen, Enhanced phosphoinositide 3-kinase(p110alpha) activity prevents diabetes-induced cardiomyopathy and superoxide generation in a mouse model of diabetes, Diabetologia 55 (12) (2012) 3369–3381.
[11] E. Plante, A. Menaouar, B.A. Danalache, T.L. Broderick, M. Jankowski, J. Gutkowska, Treatment with brain natriuretic peptide prevents the development of cardiac dysfunction in obese diabetic db/db mice, Diabetologia 57 (6) (2014) 1257–1267.
[12] P. Mishra, D.C. Chan, Mitochondrial dynamics and inheritance during cell division, development and disease, Nat. Rev. Mol. Cell Biol. 15 (10) (2014) 634–646.
[13] C. Vasquez-Trincado, I. Garcia-Carvajal, C. Pennanen, V. Parra, J.A. Hill, B. A. Rothermel, S. Lavandero, Mitochondrial dynamics, mitophagy and cardiovascular disease, J. Physiol. 594 (3) (2016) 509–525.
[14] M. Ding, N. Feng, D. Tang, J. Feng, Z. Li, M. Jia, Z. Liu, X. Gu, Y. Wang, F. Fu, J. Pei, Melatonin prevents Drp1-mediated mitochondrial fission in diabetic hearts through SIRT1-PGC1alpha pathway, J. Pineal Res. 65 (2) (2018), e12491.
[15] J. Gu, S. Wang, H. Guo, Y. Tan, Y. Liang, A. Feng, Q. Liu, C. Damodaran, Z. Zhang, B.B. Keller, C. Zhang, L. Cai, Inhibition of p53 prevents diabetic cardiomyopathy by preventing early-stage apoptosis and cell senescence, reduced glycolysis, and impaired angiogenesis, Cell Death Dis. 9 (2) (2018) 82.
[16] L. Hu, M. Ding, D. Tang, E. Gao, C. Li, K. Wang, B. Qi, J. Qiu, H. Zhao, P. Chang, F. Fu, Y. Li, Targeting mitochondrial dynamics by regulating Mfn2 for therapeutic intervention in diabetic cardiomyopathy, Theranostics 9 (13) (2019) 3687–3706.
[17] M. Ding, C. Liu, R. Shi, M. Yu, K. Zeng, J. Kang, F. Fu, M. Mi, Mitochondrial fusion promoter restores mitochondrial dynamics balance and ameliorates diabetic

cardiomyopathy in an optic atrophy 1-dependent way, Acta Physiol. 229 (1) (2020), e13428.
[18] M. Yu, N.D. Nguyen, Y. Huang, D. Lin, T.N. Fujimoto, J.M. Molkentine, A. Deorukhkar, Y. Kang, F.A. San Lucas, C.J. Fernandes, E.J. Koay, S. Gupta, H. Ying, A.C. Koong, J.M. Herman, J.B. Fleming, A. Maitra, C.M. Taniguchi, Mitochondrial fusion exploits a therapeutic vulnerability of pancreatic cancer, JCI Insight 5 (16) (2019), e126915.
[19] M. Gao, J. Wang, W. Wang, J. Liu, C.W. Wong, Phosphatidylinositol 3-kinase affects mitochondrial function in part through inducing peroxisome proliferator-activated receptor gamma coactivator-1beta expression, Br. J. Pharmacol. 162 (4) (2011) 1000–1008.
[20] X. Zhang, H. Xie, P. Chang, H. Zhao, Y. Xia, L. Zhang, X. Guo, C. Huang, F. Yan, L. Hu, C. Lin, Y. Li, Z. Xiong, X. Wang, G. Li, L. Deng, S. Wang, L. Tao, Glycoprotein M6B interacts with TbetaRI to activate TGF-beta-smad2/3 signaling and promote smooth muscle cell differentiation, Stem Cell. 37 (2) (2019) 190–201.
[21] S. Zhang, Y. Tu, Y.M. Sun, Y. Li, R.M. Wang, Y. Cao, L. Li, L.C. Zhang, Z.B. Wang, Swiprosin-1 deficiency impairs macrophage immune response of septic mice, JCI Insight 3 (3) (2018), e95396.
[22] J. Zielonka, M. Hardy, B. Kalyanaraman, HPLC study of oxidation products of hydroethidine in chemical and biological systems: ramifications in superoxide measurements, Free Radic. Biol. Med. 46 (3) (2009) 329–338.
[23] Z. Zhang, J. Yan, A.B. Bowman, M.R. Bryan, R. Singh, M. Aschner, Dysregulation of TFEB contributes to manganese-induced autophagic failure and mitochondrial dysfunction in astrocytes, Autophagy 16 (8) (2020) 1506–1523.
[24] S. Steven, M. Oelze, A. Hanf, S. Kroller-Schon, F. Kashani, S. Roohani, P. Welschof, M. Kopp, U. Godtel-Armbrust, N. Xia, H. Li, E. Schulz, K.J. Lackner, L. Wojnowski, S.P. Bottari, P. Wenzel, E. Mayoux, T. Munzel, A. Daiber, The SGLT2 inhibitor empagliflozin improves the primary diabetic complications in ZDF rats, Redox Biol. 13 (2017) 370–385.
[25] K. Vujacic-Mirski, K. Bruns, S. Kalinovic, M. Oelze, S. Kroller-Schon, S. Steven, M. Mojovic, B. Korac, T. Munzel, A. Daiber, Development of an analytical assay for electrochemical detection and quantification of protein-bound 3-nitrotyrosine in biological samples and comparison with classical, Antibody-Based Methods, Antioxidants (Basel) 9 (5) (2020) 388.
[26] F. Fu, C. Liu, R. Shi, M. Li, M. Zhang, Y. Du, Q. Wang, J. Li, G. Wang, J. Pei, M. Ding, Punicalagin protects against diabetic cardiomyopathy by promoting opa1-mediated mitochondrial fusion via regulating PTP1B-Stat3 pathway, Antioxidants Redox Signal. 35 (8) (2021) 618–641.
[27] C. Wang, M. Shi, J. Ji, Q. Cai, J. Jiang, H. Zhang, Z. Zhu, J. Zhang, A self-enforcing HOXA11/Stat3 feedback loop promotes stemness properties and peritoneal metastasis in gastric cancer cells, Theranostics 9 (25) (2019) 7628–7647.
[28] R. Ni, T. Cao, S. Xiong, J. Ma, G.C. Fan, J.C. Lacefield, Y. Lu, S. Le Tissier, T. Peng, Therapeutic inhibition of mitochondrial reactive oxygen species with mito-TEMPO reduces diabetic cardiomyopathy, Free Radic. Biol. Med. 90 (2016) 12–23.
[29] M.C. Asensio-Lopez, F. Soler, J. Sanchez-Mas, D. Pascual-Figal, F. Fernandez-Belda, A. Lax, Early oxidative damage induced by doxorubicin: source of production, protection by GKT137831 and effect on Ca(2+) transporters in HL-1 cardiomyocytes, Arch. Biochem. Biophys. 594 (2016) 26–36.
[30] L. Wang, S.A. Frizzell, X. Zhao, M.T. Gladwin, Normoxic cyclic GMP-independent oxidative signaling by nitrite enhances airway epithelial cell proliferation and wound healing, Nitric Oxide 26 (4) (2012) 203–210.
[31] R.Q. Chang, J. Shao, Y.H. Meng, J. Wang, D.J. Li, M.Q. Li, Decidual RANKL/RANK interaction promotes the residence and polarization of TGF-beta1-producing regulatory gammadelta T cells, Cell Death Dis. 10 (2) (2019) 113.
[32] S. Lei, W. Su, Z.Y. Xia, Y. Wang, L. Zhou, S. Qiao, B. Zhao, Z. Xia, M.G. Irwin, Hyperglycemia-induced oxidative stress abrogates remifentanil preconditioning-mediated cardioprotection in diabetic rats by impairing caveolin-3-modulated PI3K/akt and JAK2/STAT3 signaling, Oxid. Med. Cell. Longev. (2019), 9836302, 2019.
[33] R. Xue, S. Lei, Z.Y. Xia, Y. Wu, Q. Meng, L. Zhan, W. Su, H. Liu, J. Xu, Z. Liu, B. Zhou, Z. Xia, Selective inhibition of PTEN preserves ischaemic post-conditioning cardioprotection in STZ-induced Type 1 diabetic rats: role of the PI3K/Akt and JAK2/STAT3 pathways, Clin. Sci. (Lond.) 130 (5) (2016) 377–392.
[34] D.A. Rosen, S.M. Seki, A. Fernandez-Castaneda, R.M. Beiter, J.D. Eccles, J. A. Woodfolk, A. Gaultier, Modulation of the sigma-1 receptor-IRE1 pathway is beneficial in preclinical models of inflammation and sepsis, Sci. Transl. Med. 11 (478) (2019) eaax3130.
[35] X. Liu, Y. Cheng, J. Yang, S. Qin, X. Chen, X. Tang, X. Zhou, T.J. Krall, C. Zhang, Flank sequences of miR-145/143 and their aberrant expression in vascular disease: mechanism and therapeutic application, J. Am. Heart Assoc. 2 (6) (2013), e000407.
[36] Y.M. Lee, J.P. Park, K.T. Lim, S.J. Lee, Intestinal epithelial cell apoptosis due to a hemolytic toxin from Vibrio vulnificus and protection by a 36kDa glycoprotein from Rhus verniciflua Stokes, Food Chem. Toxicol. 125 (2019) 46–54.
[37] D. Toullec, P. Pianetti, H. Coste, P. Bellevergue, T. Grand-Perret, M. Ajakane, V. Baudet, P. Boissin, E. Boursier, F. Loriolle, et al., The bisindolylmaleimide GF 109203X is a potent and selective inhibitor of protein kinase C, J. Biol. Chem. 266 (24) (1991) 15771–15781.
[38] Z. Harhous, G.W. Booz, M. Ovize, G. Bidaux, M. Kurdi, An update on the multifaceted roles of STAT3 in the heart, Front Cardiovasc Med 6 (2019) 150.
[39] V. Leidgens, J. Proske, L. Rauer, S. Moeckel, K. Renner, U. Bogdahn, M. J. Riemenschneider, M. Proescholdt, A. Vollmann-Zwerenz, P. Hau, C. Seliger, Stattic and metformin inhibit brain tumor initiating cells by reducing STAT3-phosphorylation, Oncotarget 8 (5) (2017) 8250–8263.
[40] A. Gorbe, Z. Giricz, A. Szunyog, T. Csont, D.S. Burley, G.F. Baxter, P. Ferdinandy, Role of cGMP-PKG signaling in the protection of neonatal rat cardiac myocytes subjected to simulated ischemia/reoxygenation, Basic Res. Cardiol. 105 (5) (2010) 643–650.
[41] D.S. Burley, G.F. Baxter, B-type natriuretic peptide at early reperfusion limits infarct size in the rat isolated heart, Basic Res. Cardiol. 102 (6) (2007) 529–541.
[42] C. Liu, Y. Han, X. Gu, M. Li, Y. Du, N. Feng, J. Li, S. Zhang, L.N. Maslov, G. Wang, J. Pei, F. Fu, M. Ding, Paeonol promotes Opa1-mediated mitochondrial fusion via activating the CK2alpha-Stat3 pathway in diabetic cardiomyopathy, Redox Biol. 46 (2021), 102098.
[43] G.W. Dorn, 2nd, evolving concepts of mitochondrial dynamics, Annu. Rev. Physiol. 81 (2019) 1–17.
[44] V. Parra, H.E. Verdejo, M. Iglewski, A. Del Campo, R. Troncoso, D. Jones, Y. Zhu, J. Kuzmicic, C. Pennanen, C. Lopez-Crisosto, F. Jana, J. Ferreira, E. Noguera, M. Chiong, D.A. Bernlohr, A. Klip, J.A. Hill, B.A. Rothermel, E.D. Abel, A. Zorzano, S. Lavandero, Insulin stimulates mitochondrial fusion and function in cardiomyocytes via the Akt-mTOR-NFkappaB-Opa-1 signaling pathway, Diabetes 63 (1) (2014) 75–88.
[45] Z. Song, H. Chen, M. Fiket, C. Alexander, D.C. Chan, OPA1 processing controls mitochondrial fusion and is regulated by mRNA splicing, membrane potential, and Yme1L, J. Cell Biol. 178 (5) (2007) 749–755.
[46] M. Picard, O.S. Shirihai, B.J. Gentil, Y. Burelle, Mitochondrial morphology transitions and functions: implications for retrograde signaling? Am. J. Physiol. Regul. Integr. Comp. Physiol. 304 (6) (2013) R393–R406.
[47] S. Cipolat, T. Rudka, D. Hartmann, V. Costa, L. Serneels, K. Craessaerts, K. Metzger, C. Frezza, W. Annaert, L. D'Adamio, C. Derks, T. Dejaegere, L. Pellegrini, R. D'Hooge, L. Scorrano, B. De Strooper, Mitochondrial rhomboid PARL regulates cytochrome c release during apoptosis via OPA1-dependent cristae remodeling, Cell 126 (1) (2006) 163–175.
[48] S.B. Ong, S.B. Kalkhoran, S. Hernandez-Resendiz, P. Samangouei, S.G. Ong, D. J. Hausenloy, Mitochondrial-shaping proteins in cardiac Health and disease - the long and the short of it, Cardiovasc. Drugs Ther. 31 (1) (2017) 87–107.
[49] K. Miyashita, H. Itoh, H. Tsujimoto, N. Tamura, Y. Fukunaga, M. Sone, K. Yamahara, D. Taura, M. Inuzuka, T. Sonoyama, K. Nakao, Natriuretic peptides/cGMP/cGMP-dependent protein kinase cascades promote muscle mitochondrial biogenesis and prevent obesity, Diabetes 58 (12) (2009) 2880–2892.
[50] Y. Sun, T. Deng, N. Lu, M. Yan, X. Zheng, B-type natriuretic peptide protects cardiomyocytes at reperfusion via mitochondrial calcium uniporter, Biomed. Pharmacother. 64 (3) (2010) 170–176.
[51] X. Kong, X. Wang, W. Xu, S. Behera, G. Hellermann, A. Kumar, R.F. Lockey, S. Mohapatra, S.S. Mohapatra, Natriuretic peptide receptor a as a novel anticancer target, Cancer Res. 68 (1) (2008) 249–256.
[52] M. Zhang, D.A. Kass, Phosphodiesterases and cardiac cGMP: evolving roles and controversies, Trends Pharmacol. Sci. 32 (6) (2011) 360–365.
[53] J. Inserte, D. Garcia-Dorado, The cGMP/PKG pathway as a common mediator of cardioprotection: translatability and mechanism, Br. J. Pharmacol. 172 (8) (2015) 1996–2009.
[54] C. Matyas, B.T. Nemeth, A. Olah, L. Hidi, E. Birtalan, D. Kellermayer, M. Ruppert, S. Korkmaz-Icoz, G. Kokeny, E.M. Horvath, G. Szabo, B. Merkely, T. Radovits, The soluble guanylate cyclase activator cinaciguat prevents cardiac dysfunction in a rat model of type-1 diabetes mellitus, Cardiovasc. Diabetol. 14 (2015) 145.
[55] V. Borutaite, R. Morkuniene, O. Arandarcikaite, A. Jekabsone, J. Barauskaite, G. C. Brown, Nitric oxide protects the heart from ischemia-induced apoptosis and mitochondrial damage via protein kinase G mediated blockage of permeability transition and cytochrome c release, J. Biomed. Sci. 16 (2009) 70.
[56] L.M. Yu, W.C. Di, X. Dong, Z. Li, Y. Zhang, X.D. Xue, Y.L. Xu, J. Zhang, X. Xiao, J. S. Han, Y. Liu, Y. Yang, H.S. Wang, Melatonin protects diabetic heart against ischemia-reperfusion injury, role of membrane receptor-dependent cGMP-PKG activation, Biochim. Biophys. Acta, Mol. Basis Dis. 1864 (2) (2018) 563–578.
[57] V. Malek, N. Sharma, A.B. Gaikwad, Histone acetylation regulates natriuretic peptides and neprilysin gene expressions in diabetic cardiomyopathy and nephropathy, Curr. Mol. Pharmacol. 12 (1) (2019) 61–71.
[58] E. Shen, X. Diao, X. Wang, R. Chen, B. Hu, MicroRNAs involved in the mitogen-activated protein kinase cascades pathway during glucose-induced cardiomyocyte hypertrophy, Am. J. Pathol. 179 (2) (2011) 639–650.
[59] O. Nakagawa, Y. Ogawa, H. Itoh, S. Suga, Y. Komatsu, I. Kishimoto, K. Nishino, T. Yoshimasa, K. Nakao, Rapid transcriptional activation and early mRNA turnover of brain natriuretic peptide in cardiocyte hypertrophy. Evidence for brain natriuretic peptide as an "emergency" cardiac hormone against ventricular overload, J. Clin. Invest. 96 (3) (1995) 1280–1287.
[60] R. Kerkela, J. Ulvila, J. Magga, Natriuretic peptides in the regulation of cardiovascular physiology and metabolic events, J. Am. Heart Assoc. 4 (10) (2015), e002423.
[61] C. Bielmann, S. Rignault-Clerc, L. Liaudet, F. Li, T. Kunieda, C. Sogawa, T. Zehnder, B. Waeber, F. Feihl, N. Rosenblatt-Velin, Brain natriuretic peptide is able to stimulate cardiac progenitor cell proliferation and differentiation in murine hearts after birth, Basic Res. Cardiol. 110 (1) (2015) 455.
[62] S. Wu, Q. Lu, Y. Ding, Y. Wu, Y. Qiu, P. Wang, X. Mao, K. Huang, Z. Xie, M.H. Zou, Hyperglycemia-driven inhibition of AMP-activated protein kinase alpha2 induces diabetic cardiomyopathy by promoting mitochondria-associated endoplasmic reticulum membranes in vivo, Circulation 139 (16) (2019) 1913–1936.